PROCEEDINGS OF THE ROYAL SOCIETY A MATHEMATICAL, PHYSICAL & ENGINEERING SCIENCES

The Clifford Paterson Lecture, 1986. Limits of Thin-Film Microfabrication

A. N. Broers

Proc. R. Soc. Lond. A 1988 **416**, 1-42
doi: 10.1098/rspa.1988.0024

Proc. R. Soc. Lond. A **416**, 1–42 (1988)
Printed in Great Britain

The Clifford Paterson Lecture, 1986

Limits of thin-film microfabrication

By A. N. Broers, F.R.S.

Engineering Department, University of Cambridge, Trumpington Street, Cambridge CB2 1PZ, U.K.

(*Lecture delivered* 2 *July* 1986 – *Typescript received* 21 *August* 1987)

[Plates 1 and 2]

Thin-film microfabrication techniques are used to make semiconductor integated circuits, integrated optical devices, thin-film magnetic recording heads, and a variety of other devices of commercial and scientific interest. The dimensional accuracy that can be achieved with the techniques frequently determines whether or not devices can be built, and it is almost always a major influence on device performance. In addition, the commercial viability of most devices depends on the cost, and the speed of the fabrication methods. This lecture discusses the practical and theoretical limits of thin-film fabrication processes. Emphasis is placed on ultraviolet light, X-ray, electron and ion lithographies. Ultimately, it is possible to build structures with dimensions of only a few atomic diameters. These so-called 'nanostructures' are being used in a variety of scientific investigations. Their fabrication, which is described, illustrates the limits to fabrication capability.

1. Introduction

Thin-film microfabrication processes are used to make many different devices. The most important are integrated circuits, known colloquially as chips, but there are many others of significance including optoelectronic components, thin-film magnetic recording heads, surface-wave devices and structures so small that they can be used by physicists to probe quantum effects in electronic conduction. The range of sizes encompassed by these devices and by the techniques used to fabricate and examine them is shown in figure 1.

In this lecture, I describe the imaging methods that define the resist patterns used in thin-film microfabrication. The resist patterns act as masks or templates for subsequent steps, such as etching, that produce the final structures. In some cases these subsequent steps affect the resolution of the fabrication process, but generally it is the resist imaging methods that set the resolution limits.

The motivation for miniaturizing integrated circuits is that smaller devices operate faster, consume less power and cost less. The cost scales approximately with the square of the size, and the performance with the size. The power per circuit is reduced enough with size to avoid overheating. The revolution in information

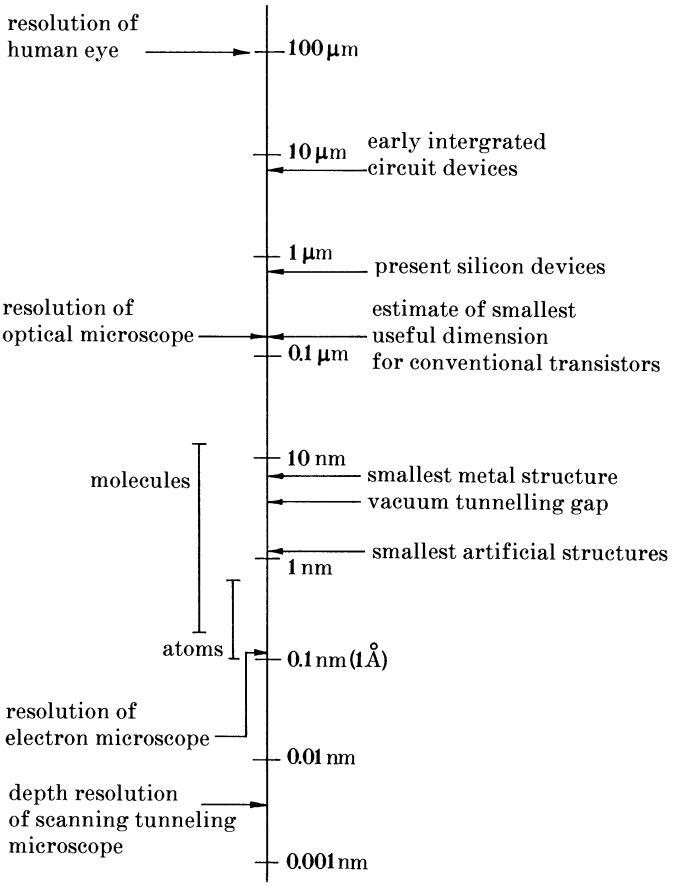

FIGURE 1. Size scale for microstructures, microfabrication methods and microscopy.

technology that has occurred over the past twenty five years has largely been a result of the successful miniaturization of integrated circuits. Dimensions have been reduced by a factor of about ten, from 10 to 1 μm, and it is thought that another factor of ten can be accomplished without inventing new devices. As the density of components reaches the level at which whole systems can be integrated on a single chip, the cost and performance improvements are even greater than the scaling factors indicate. This is because packaging becomes cheaper and interconnection distances become shorter. Advances in all these areas are likely to continue through the end of the century suggesting that the revolution in information processing will continue at the same pace at least until then.

The fabrication methods used to make chips must be economical because the motivation for miniaturizing integrated circuits is largely economical. For example, exposure speed must be fast, and equipment cost low. It it particularly difficult to achieve the latter for electron-beam and X-ray lithographies. On the other hand, for making a small number of nanostructures (structures smaller than 0.1 μm) for physics experiments, the cost is not as important as the ultimate

resolution. Both the economic and the ultimate limits are reviewed in this lecture. I will first discuss the practical aspects of integrated circuit fabrication and then the factors that determine the ultimate size of the structures that can be made.

2. Basic fabrication processes and ultimate resolution

Figure 2 shows three of the basic ways of making thin-film structures. In each case the size of the structures depends on the resolution of the resist pattern and hence on the imaging method used to expose the resist. With the highest-resolution resists, resolution is not set by the resist but by the resolution of the exposing tool, or by scattering or delocalization of the energy of the exposing radiation in the resist or sample. Resist contrast and resist development can, none the less, affect the dimensional accuracy of resist patterns.

Figure 3 shows fabrication methods that avoid the use of resists by making use of sharp steps on surfaces. They have been used selectively in the fabrication of both integrated circuits and scientific devices. The minimum size of the structure

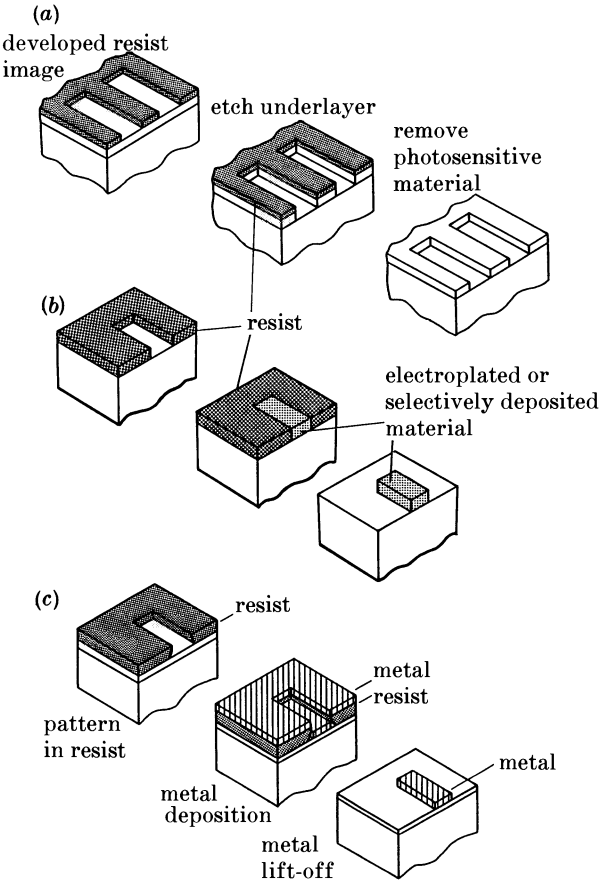

Figure 2. Three basic ways to make thin-film structures. (*a*) subtractive etching, (*b*) plating or selective deposition and (*c*) lift-off.

PROCEEDINGS OF THE ROYAL SOCIETY A MATHEMATICAL, PHYSICAL & ENGINEERING SCIENCES

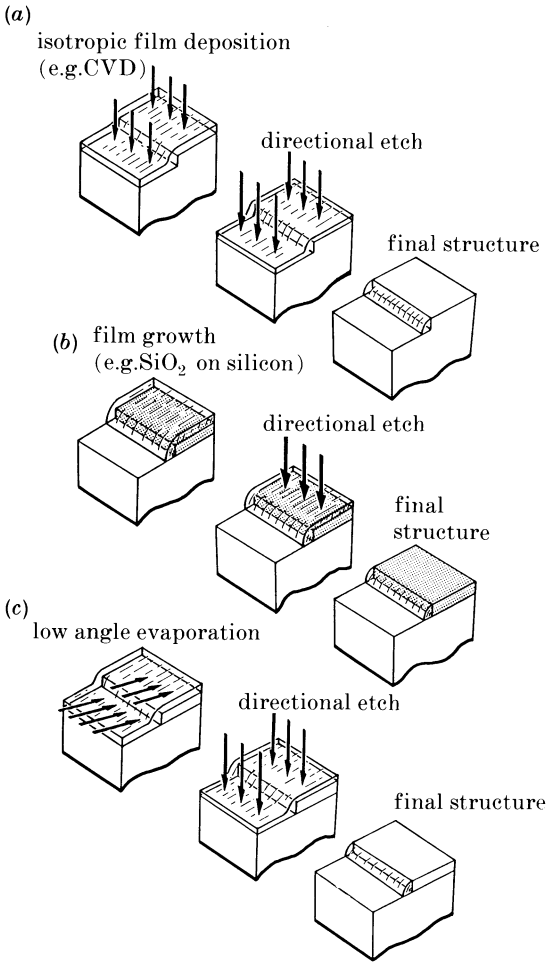

FIGURE 3. Fabrication methods that make use of steps on the surface of the sample to fabricate thin wires or spacers.

is set by the sharpness of the step and by the ability to control the thickness of the deposited film. It is possible to produce structures smaller than 0.1 μm in size but the pattern shapes that can be formed are obviously limited.

In all cases the perfection of the final structures depends on the perfection of the thin films of which they are made. Ideally, epitaxial films are needed. When etching is used to make the final structures, it may 'damage' the regions adjacent to the edges of the structures and thereby limit their useful size.

Most thin-film devices require several fabrication steps and the pattern for each step must be accurately positioned with respect to the previous patterns. Errors in the position of one pattern with respect to another are known as overlay errors. They consist of alignment errors, that is errors in the relative position of the alignment mark on the two patterns, and distortion errors. The latter may arise in the mask and/or the sample, or be produced by the imaging tool. For integrated

circuits, hundreds of measurements are made of the different errors and the overlay accuracy assessed statistically. Overlay data are then combined with data on errors in the size of pattern features to decide upon the final size and density of the circuits. Typically, integrated circuit devices are designed to be tolerant to errors two to three times greater than might be measured in a few laboratory experiments. It is frequently the overlay accuracy that determines the minimum size of the components and not the resolution of the fabrication process.

3. Ultraviolet shadow printing

Contact printing with UV light is no longer used to make integrated circuits, despite its high resolution compared with other optical methods, because of defects created when the mask and wafer accidentally touch each other. It is still used to fabricate simpler structures that are more tolerant to defects, and larger structures where a big enough gap can be left between the mask and the wafer to avoid mask to sample contact. When a gap is left, the process is called proximity printing. In fact, contact printing is really proximity printing because of the thickness of the resist.

Minimum linewidth in proximity printing is set by Fresnel diffraction between the mask and the bottom of the resist. This is shown qualitatively in figure 4. A

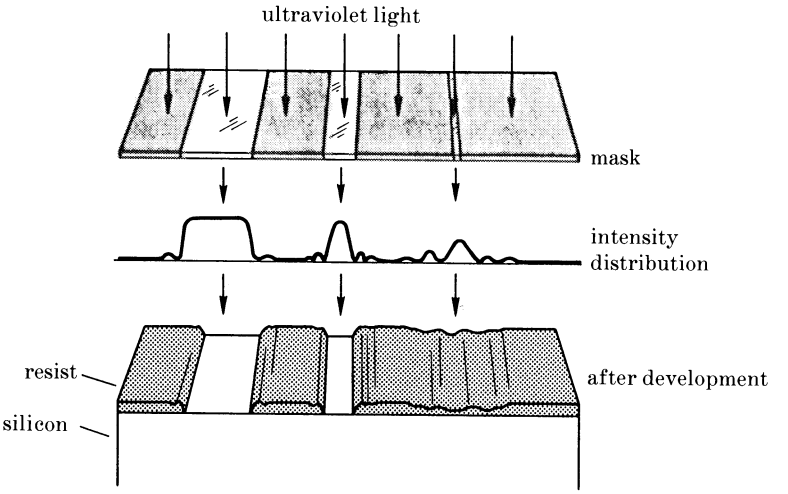

Figure 4. Proximity printing with UV light. Resolution is limited by Fresnel diffraction between the mask and the sample.

'rule-of-thumb' approximation for the minimum linewidth is that it is equal to $(\lambda g)^{\frac{1}{2}}$ μm, where λ is the wavelength of the exposing radiation in micrometres, and g is the gap between the mask and the bottom of the resist in micrometres; $(\lambda g)^{\frac{1}{2}}$ is the minimum linewidth at which the intensity at the centre of the line approaches that of the background radiation. It is an optimistic approximation because it is difficult to control linewidth in this size régime. The exposure dose at the centre of a line varies rapidly from below, to 70% above, the background level

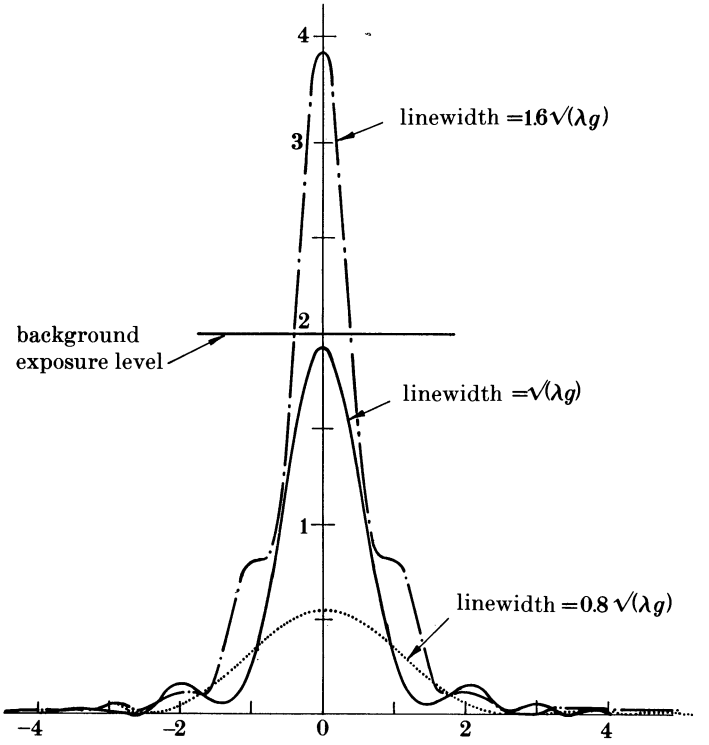

FIGURE 5. Intensity profile for linewidths above and below the nominal minimum acceptable linewidth of $(\lambda g)^{\frac{1}{2}}$ for proximity printing.

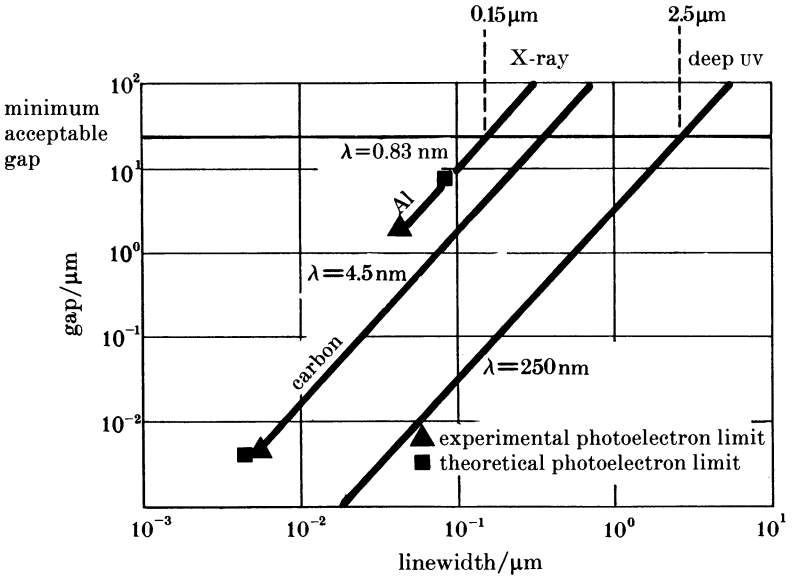

FIGURE 6. Linewidth against gap for contact or proximity printing.

for linewidths immediately above and below this size. Figure 5 shows the intensity profile for linewidths above and below $(\lambda g)^{\frac{1}{2}}$.

Linewidth against gap for proximity printing is plotted in figure 6. Ultimately, linewidth is limited only by the thickness of the imaging layer. For example, it should be possible with UV light to produce 250 nm dimensions in 100 nm thick resist provided that intimate contact is maintained between mask and resist. The case for X-rays shown in figure 6 is discussed next.

4. X-RAY LITHOGRAPHY

4.1. *General*

The resolution problem of proximity printing is largely overcome if X-rays, with their much shorter wavelength, are used instead of UV light. Proximity printing with soft X-rays is known as X-ray lithography (Spears & Smith 1972). It is the only practicable method for using X-rays for microlithography because the field size and resolution of X-ray lenses are not yet good enough for projection imaging.

Relatively soft X-rays (wavelength between 0.4 nm and 5 nm) are used so that sufficient energy is absorbed in the resist. At these wavelengths diffraction effects are negligible down to linewidths of about 0.2 μm for a practicable mask to wafer spacing of 50 μm. The mask can no longer be made on a quartz plate because such a plate would absorb the soft X-rays. Instead it is formed on a thin (less than 10 μm) membrane of materials such as silicon, silicon carbide, polyimide or a combination of two materials. The absorber is a metal film with high atomic mass patterned with scanning electron-beam lithography.

X-ray lithography offers higher resolution than foreseeable optical cameras and lower cost than scanning electron-beam lithography. It produces sharper exposure distributions in thick resist layers than either of these alternatives except for dimensions of less than 0.1 μm where electrons produce higher ratios of resist thickness to minimum linewidth. Figure 7, plate 1, shows the type of high-aspect-ratio resist pattern produced by X-rays (Heuberger 1986*a*). X-ray exposure is also relatively unaffected by the small, low-atomic-mass particles, such as skin flakes, that are frequently 'printed' in optical lithograpy.

Difficulties with X-ray lithography are that the mask is fragile and may not be dimensionally stable, that exposure speed is marginal and that present alignment methods do not offer better accuracy than is achieved with optical lithography. None of these are fundamental but their solution is likely to take several years.

4.2. *Resolution*

Two factors set the resolution for X-ray lithography; (1) Fresnel diffraction between the mask and the surface of the sample, and (2) the range of the photoelectrons formed when the X-ray photons are absorbed in the resist.

The same diffraction criterion used above for UV radiation can be applied to X-rays and from figure 6 it can be seen, for example, that the minimum linewidth set by diffraction for 0.8 nm X-rays and a gap of 50 μm, is 0.15 μm.

The photoelectron range can be estimated from the Gruen dose–depth relation

for electrons (Gruen 1957) although this relation has only been confirmed for energies between 5 and 54 keV. None the less, it predicts the resolution for a typical resist such as PMMA (density 1.2 g cm^{-3}) to within a factor of about two (Spiller & Feder 1977). The minimum linewidth is assumed to be equal to the Gruen range R_G, where $R_G \approx 10^{-23}\lambda^{-1.75}$ m, and λ is the wavelength in micrometres of the exposing radiation. For example, $R_G = 56$ nm for $\lambda = 1$ nm.

For linewidths less than about 100 nm, a compromise has to be made between the need to use short wavelength X-rays to reduce the effects of diffraction, and the need to use long wavelength (e.g. 4.5 nm) X-rays to reduce the photoelectron range. Linewidths below a few tens of nanometres will probably only be possible with masking layers that are formed directly on the resist surface, thereby minimizing the mask to sample gap but eliminating the ability to produce many exposures from a single mask. In these cases, as will be discussed later, direct electron-beam exposure is better. In any case, the resolution of X-ray exposure is set by the electron beam lithography used to make the mask.

4.3. *Throughput*

The only X-ray source that presently provides exposure speed comparable to that of optical cameras is the electron-synchrotron storage ring (figure 8). For several years physicists have been using storage rings because they are the

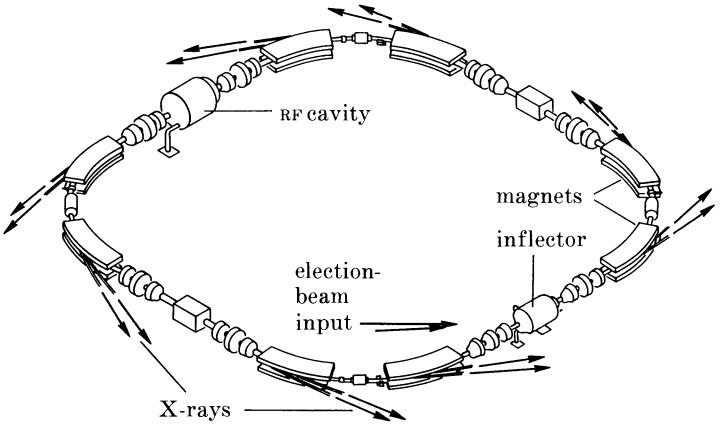

FIGURE 8. Electron-synchrotron storage ring of the type used in exploratory X-ray lithography experiments. A high current (more than 100 mA) electron beam with an energy between 500 MeV and 2 GeV circulates in the ring. The beam radiates 'white' radiation with wavelengths extending into the soft X-ray régime when it is deflected by the bending magnets.

'brightest' source of short-wavelength light. A storage ring consists of a circular stainless-steel vacuum tube in which electrons circulate at speeds very close to the speed of light. The electrons are injected into the ring from an accelerator, and their energy is increased to a nominal value and maintained then by the microwave cavity that forms part of the ring. They are held in the circular orbit by magnets. Each time the electrons are deflected by one of the magnets they emit

an intense beam of radiation with a range of wavelengths that extends from that of visible light to that of hard X-rays.

At first it would seem difficult to understand how an expensive device like a storage ring could be economical for manufacturing microcircuits. A storage ring costs between £5M and £15M. The answer lies in the vast total X-ray flux that emanates from the ring. Enough radiation is emitted at each of the typically sixteen bending magnets to expose 40 wafers per hour of diameter 125 mm, a production rate similar to that of today's optical step-and-repeat cameras. Therefore, fully utilized, a storage ring could produce the equivalent of about sixteen projection cameras. A step-and-repeat camera costs about £0.5M, so provided that one uses all the storage ring ports, the ring becomes cost competitive and of course can produce smaller devices.

Compact electron-synchrotron storage rings that use superconducting rather than normal magnets offer similar output to the full-size rings but their smaller size should make them even more economical for production use. Figure 9 shows a compact ring that is designed to supply radiation to about twelve exposure stations. Compact rings should be small enough to be installed as complete assembled units thereby avoiding the prolonged assembly time needed for full-size rings.

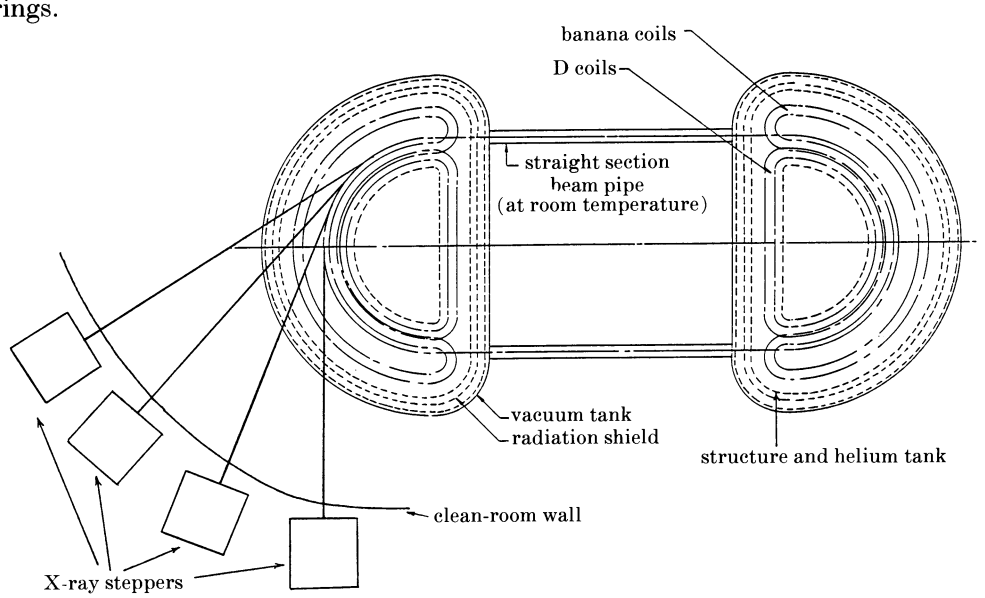

FIGURE 9. Configuration for X-ray lithography with a compact electron storage ring. Race-track, rather than circular storage rings, were first proposed by Oxford Instruments.

A major difficulty with storage rings is that failure of the ring disables many exposure stations. The possibility of having two rings that would serve a single set of exposure stations has been considered but the practical difficulties of this approach are obvious.

Laser excited plasma sources, and pinched plasma (sometimes called plasma focus) sources are possible alternatives to the storage ring but their output is

currently ten to a hundred times lower (Heuberger 1986*b*). Electron bombardment sources have been used for most X-ray lithography experiments until now but they also produce too little output for production use.

A comparison between the different sources is shown in table 1.

TABLE 1. X-RAY SOURCES; CHARACTERISTICS AND THROUGHPUT

(4 cm × 4 cm exposure field; mask–wafer gap, 50 μm; control of gap, 5 μm; run-out displacement, 0.25 μm.)

	X-ray tube	laser plasma	storage ring
divergence/mrad	~50	~50	~5
distance source–mask/m	0.4	0.4	4
source diameter/mm	3	0.1	0.5
penumbral blurring/μm	~0.4	0.015	negligible
spectrum	line	line	broad band 0.4–2 nm
total power/(mW cm^{-2})	> 1	> 1	> 100
(exposure time/field)/(100 mJ^{-1} cm s)	100	100	1
20 cm wafer throughput/h^{-1}	1	1	40

4.4. *Masks, overlay accuracy and mask distortion*

Work is still needed to perfect the thin-membrane X-ray masks, in particular to reduce distortion to acceptable levels, and to obtain adequate definition in the absorber pattern, which typically has to be 1 μm thick. Distortion is minimized by adjusting stress levels in the membrane and the absorber pattern. The aim is to have the membrane under small tensile stress so that it does not wrinkle, and to make the absorber free of stress so that there are no distortions due to local variations in absorber coverage.

With point sources (electron bombardment, laser–plasma or plasma discharge) overlay errors arise not only when mask and wafer distort in the lateral plane, but when they are not flat. This problem, which gives rise to what are called 'run-out' errors, is shown in figure 10. The high aspect ratio that is needed in the absorber pattern also places requirements on the angle of incidence of the X-rays to the mask.

The way distortion and run-out errors are being tolerated is to reduce the field size and expose the wafer in a step-and-repeat manner. The penalty is a reduction in throughput that, with presently available point sources, is too great for the process to be economical for production. Throughput will only be restored by using a source with higher output such as the electron storage ring, or by finding more sensitive resists. Sensitivity approaching 1–10 mJ cm^{-2} is needed for point sources to be viable and although resists with this sensitivity are being worked on in the laboratory, they are not ready for device production.

4.5. *Summary*

X-ray lithography is perhaps the most promising method for large-scale production of devices smaller than 0.75 μm because it produces wider process

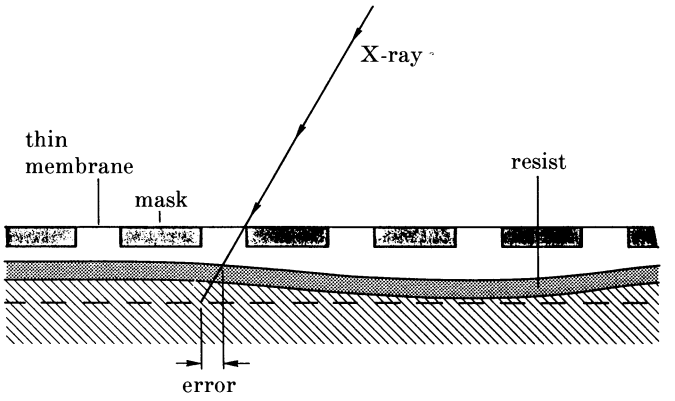

FIGURE 10. With a point source of X-rays the position of the shadow image varies with the spacing between the mask and the wafer. These errors, which add to errors due to lateral distortion of the mask and sample, frequently occur because wafers buckle during hot processing.

margins than optics and lower cost than scanning electron beams. However, no completely satisfactory source is available yet and problems remain with mask fabrication and with the control of mask distortion.

5. Ion- and electron-beam proximity printing

Ions and electrons can be used for proximity printing just as UV light and X-rays can, but it is more difficult to make the masks. Bright electron or ion sources are not needed, only sources that produce adequate current. If necessary, the beams can be scanned across the mask to complete the exposure. The angle of incidence of the beam to the mask can be altered as the beam passes over the mask to correct for distortions of the mask or the wafer.

For ions, masks have been made using a single-crystal silicon membrane and a thin gold absorber pattern. The ions channel through the membrane in the clear areas, and in the opaque areas the gold scatters the ions out of the favourable channelling direction and they are absorbed in the silicon. In channelling through the clear areas the ions are none the less scattered, and this results in image blurring of about 0.1 μm for a mask to resist separation of 15–25 μm (Parma & Hart 1987). The minimum acceptable gap from the point of view of avoiding mask and wafer touching each other is 25 μm, so this problem limits the useful linewidth to about 1 μm.

Stencil masks have to be used for electrons, because electrons would be excessively scattered by the thinnest practicable membranes. Stencil masks have been made with silicon membranes and the problem of unsupported areas falling out resolved by using two complementary masks (Ward *et al.* 1986). Features down to about 0.25 μm have been fabricated and satisfactorily replicated with electron-beam proximity printing. Stencil masks could also be used for ion-beam exposure.

The difficulties of making and repairing the masks for these particle-beam

proximity methods are severe and would seem to limit their chances of success in competition with the X-ray alternative.

6. Optical projection

6.1. *Introduction*

Most integrated circuit patterns are exposed with optical systems which project an image of a mask onto the wafer. The main advantage of projection imaging over proximity printing is that mask and sample are completely separated and defects created by contact between mask and wafer are eliminated. A second advantage is that the lens can provide demagnification allowing the mask to have larger dimensions than are required on the wafer. This makes the mask easier to fabricate, to inspect and to repair. However, some projection cameras operate at unity magnification and do not take advantage of the second attribute, because it is thought to be possible to design better projection optics for 1:1 operation.

For advanced integrated circuits with linewidths of 1 μm and below, projection lenses must operate close to diffraction limits. It is not possible to build such lenses with fields as large as an integrated circuit wafer, 100–200 mm diameter, so the image is built up in stages using one of two basic methods.

In the first, the scanning method, the mask and the wafer are moved past the lens to transfer the image from the mask to the wafer. The imaging system for a camera of this type, the Perkin Elmer Micralign 500 (the latest version is called the Micralign 600), is shown in figure 11 (Greed & Markle 1982). A crescent on the mask is imaged onto the wafer at unity magnification. As the mask and wafer are moved past the optical system, the crescent sweeps across the mask and a

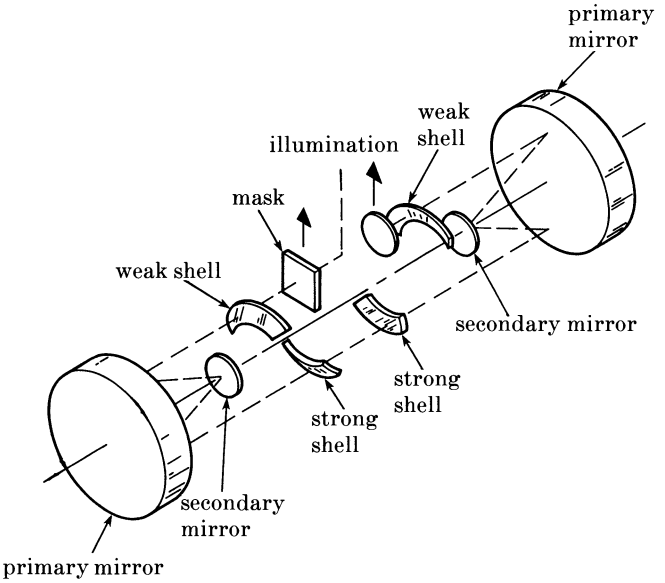

Figure 11. Ring-field optical system for Perkin Elmer 'Micralign' (registered trade mark) microcircuit camera.

complete image of the mask is built up on the wafer. The mask is critically illuminated from a curved capillary arc lamp. That is the arc is focused on to the mask by the condenser lens.

In the second, the step-and-repeat method shown in figure 12, the mask and lens are stationary and the sample is moved in steps between exposure sites. The

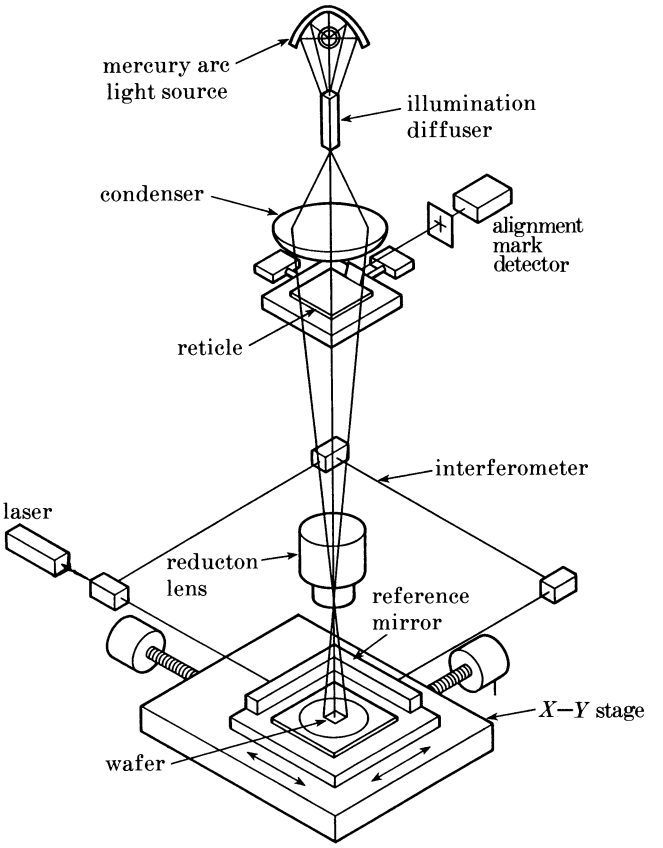

FIGURE 12. Configuration for typical 'step-and-repeat' microcircuit camera.

sample is stationary during exposure. The exposed area is typically 10–20 mm^2 and the lens demagnifies the pattern on the mask by a factor of about five. The mask is generally illuminated from a mercury arc lamp by Köhler illumination. In Köhler illumination, the mask is illuminated with divergent light and a condenser lens close to the mask collects the light and focuses an image of the arc on to the entrance pupil of the projection lens. Figure 13 shows critical and Köhler illumination.

Until now, the scanning cameras have used reflecting lenses and the step and repeat cameras have used refracting lenses but there is no fundamental reason for this, and either type of lens could be used in either type of camera. Mirror lenses appear to offer the greatest potential for improvement because they can be designed more easily to operate over a range of wavelengths. They can also be used

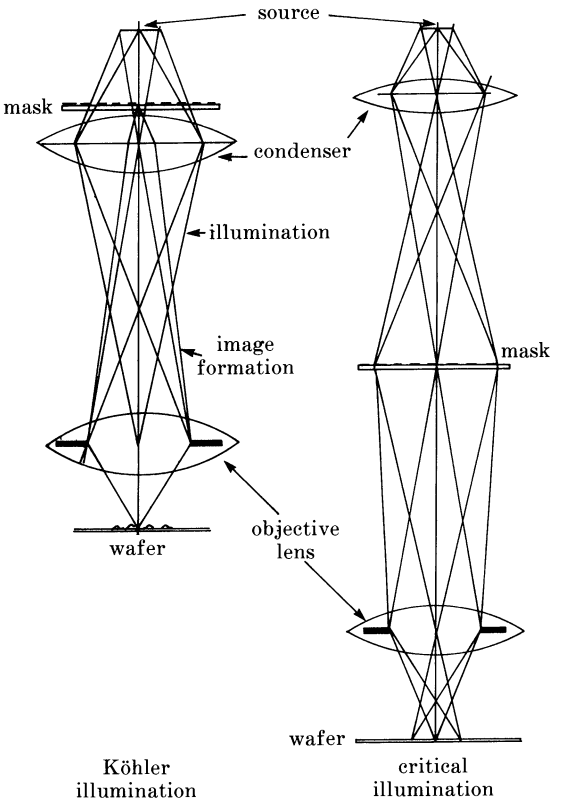

FIGURE 13. Köhler and 'critical' illumination methods for optical lithography.

at very short wavelengths (200–250 nm) where the absorption of glasses is a problem with refractive lenses.

6.2. *Resolution and depth of focus*

Resolution for a projection camera is set by the numerical aperture A_n of the projection lens (the sine of the angle that the extreme ray from the edge of the lens pupil makes with the axis at the sample) and by the wavelength of the exposing radiation. Contrast at a given resolution is given by the modulation transfer function M.T.F., where

$$\text{M.T.F.} = 2/[\pi(\phi - \cos\phi \sin\phi)],\ \phi = \arccos\{\lambda/[4L(\text{N.A.})]\}$$

and L is the linewidth in nanometres. Strictly, M.T.F. gives contrast in a sinusoidal image of a sinusoidal object, whereas an integrated circuit mask is a delta-function object but the approximation is usually adequate. An M.T.F. of 60% is considered sufficient for typical lithography applications, and 80% for cases where image size control of a tenth of the minimum linewidth is required. The acceptable limit is also a function of the reflectivity of the resist coated sample surface.

Higher contrast can be obtained for relatively large linewidths by using partly coherent illumination; that is by arranging that the image of the source only

partly fills the pupil of the projection lens. Filling of 30–50% of the pupil has proven optimum and, for example, can increase contrast from 60% for the incoherent case, to more than 80% (Offner 1979). Part coherence improves depth of focus but increases exposure time. Too high a degree of partial coherence gives rise to undesirable interference effects between lines. M.T.F. for the Micralign (0.16 N.A.) optical system and a 0.35 N.A. refractive lens are shown in figure 14. Both assume a degree of part coherence.

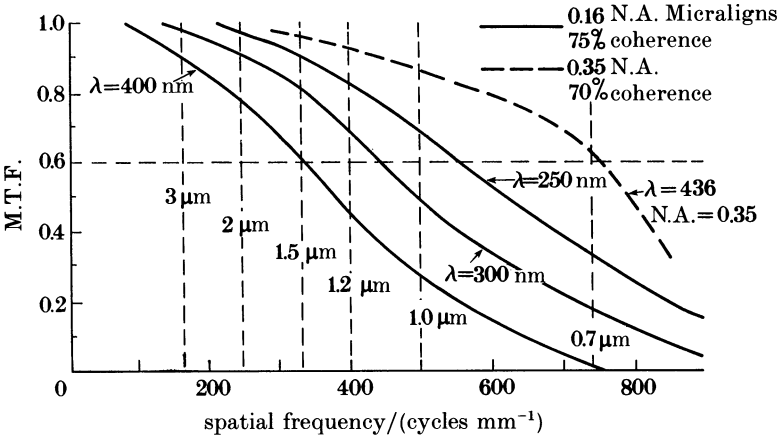

FIGURE 14. M.T.F. (modulation transfer function) for ring-field and step-and-repeat microcircuit cameras.

Depth of focus depends on substrate reflectivity, the degree of part coherence and the minimum feature size (King 1981). The classical depth of field for the incoherent case, $\pm(\lambda/2\,(\text{N.A.})^2)$, gives a reasonable approximation for a lens with a perfectly flat field, but most lenses do not have a flat field and half the depth of focus is needed frequently to tolerate this imperfection. The exposed field must therefore be flat to about $\pm(\lambda/4\,(\text{N.A.})^2)$.

Two layer resist processes in which the image is formed in a thin, flat, resist layer on top of a much thicker planarizing layer, alleviate the need for the sample to be smooth and make it easier to form high-resolution, high-aspect-ratio, resist patterns (Lin 1979; Tai *et al.* 1979; Hatzakis *et al.* 1980). With multilayer resists, satisfactory results are reported at contrast levels as low as 40%.

It is possible in principle to build microcircuit lenses with numerical aperture greater than 0.5 that operate at vacuum ultraviolet wavelengths (*ca.* 190 nm) and print linewidths approaching 0.3 μm.

The following types of camera are being developed to realize this ultimate resolution for optical projection. A summary of lenses, present and future, in terms of their resolution and field size is shown in figure 15.

6.3. *Advanced camera types*

6.3.1. *Step-and-repeat: refractive lens* (200 nm)

Lenses for step-and-repeat cameras are being built from fused silica elements so that they can operate at deep-UV wavelengths (down to 200 nm). It is thought

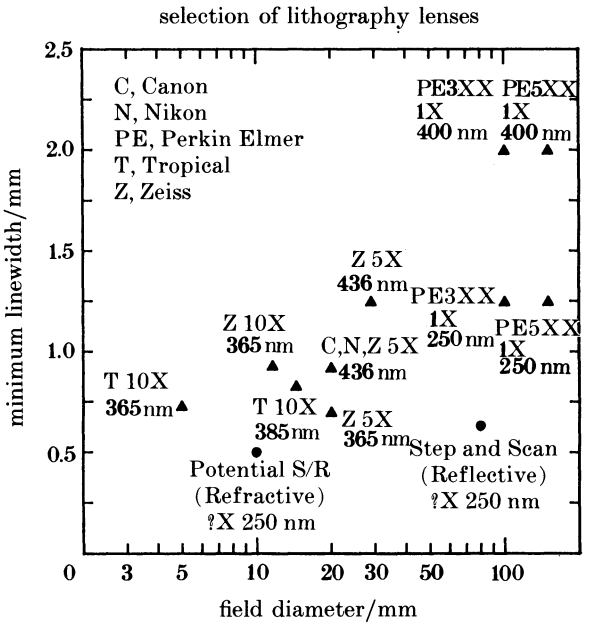

FIGURE 15. Minimum-linewidth and field-size for microcircuit lenses.

possible to avoid the need to colour-correct these lenses by using very narrow bandwidth laser illumination. This will exaggerate standing-wave interference effects but not to the extent that they are significantly worse than those encountered with the single mercury spectrum line used with today's step-and-repeat lenses. Speckle can be reduced by scanning the illumination (Pol 1987), or by using an excimer laser with a finite bandwidth (Jain *et al.* 1982).

6.3.2. *Step-and-repeat: mirror lens*

There is already one step-and-repeat camera that uses a lens whose principle elements are mirrors (Hershel & Voison 1982). At present the camera operates at a wavelength around 400 nm and produces a resolution approaching 1 μm. A similar camera operating at 200 nm would produce a theoretical resolution less than 0.5 μm.

6.3.3. *Step-and-scan*

A camera has recently been designed that retains the ring-field optical system of the full-field scanning cameras but has double the numerical aperture (Markle 1984). This has been accomplished without the need for impractically large optical elements by sacrificing the ability to expose a full water in a single scan. The length of the curved slit is reduced from the full-wafer diameter to a few centimetres. The wafer is exposed with a series of these narrower scans. The image area is about 20 mm wide and 80 mm long. The name step-and-scan has been adopted for obvious reasons. Alignment corrections are made continuously by observing reference marks in the strips between the scanned areas.

The optical system of a step-and-scan camera can be 1:1 or demagnifying and in either case the N.A. can be greater than 0.3. Operation at deep UV wavelengths has already been demonstrated with the full-field version of the same type of optical system so the step-and-scan camera should achieve a resolution approaching 0.5 μm. Predictions for throughput are similar to those for the full-wafer cameras.

6.4. *Alignment*

Projection images are aligned to previously fabricated features on the sample by examining superimposed images of the mask and the sample. The images are sometimes formed with the projection lens and sometimes with auxiliary lenses. Almost all alignment schemes suffer from the difficulty that for certain resist thicknesses and alignment mark types, light is reflected equally from the mark and from the background surface and the mark 'disappears'. To avoid this difficulty, resist thickness has to be controlled very carefully (± 10 nm is needed in some cases) or the resist removed from the marks. The alignment marks can be examined with dark-field or bright-field illumination, and often the ability to form either type of image is provided.

In the absence of the problems with alignment mark visibility, optical methods for positioning an image can be extremely precise (less than 0.1 μm). Accuracy beyond the Rayleigh criterion ($0.6\,\lambda$/N.A. cm) is possible by means of threshold detection because, in general, S/N ratios in the detected signal are favourable. Overlay accuracy over the whole sample depends on temperature control and on the ability to control mask and wafer distortion. No fundamental limits can be identified in this case.

6.5. *Outlook*

As I have already mentioned, lithography lenses for deep UV wavelengths (190–250 nm) should soon be available with N.A.s greater than 0.5. They will produce much improved resolution but will have very small depth of focus. Present lenses, such as the mirror lens in the full-field cameras of Perkin Elmer, have a numerical aperture of 0.16 and a depth of focus of 6–10 μm. Step-and-repeat camera lenses have smaller depth of focus, but expose relatively small areas so it is easier to adequately level the sample. Their depth of focus is still 2–4 μm.

Exposure wavelength of 200 nm, and 0.5 numerical aperture, will produce a resolution of 0.3 μm, but a depth of focus of only 1 μm. Vertical dimensions of integrated circuit devices will probably not scale with lateral dimensions, so the depth of focus will be no larger than the surface roughness. Multilayer resists with a planarized imaging layer will help, but the requirements for wafer flatness and levelling will become extremely severe. It seems likely that at some point around 0.5 μm linewidth the small depth of field will become intolerable and optical lithography will have to give way to electron or X-ray lithography. The ultimate limit of about 0.3 μm may therefore never be used.

PROCEEDINGS OF THE ROYAL SOCIETY A MATHEMATICAL, PHYSICAL & ENGINEERING SCIENCES

7. Scanning electron beam lithography

7.1. *Introduction*

With scanning electron-beam lithography the pattern is written directly into the resist with a finely focused electron beam. The beam is deflected and turned on and off under the control of a computer. The basic method is shown in figure 16. At first sight this is the ideal way to write integrated circuit patterns because no masks are reqiured and the resolution is beyond foreseeable needs. Unfortunately electron beam writing is at least ten times more expensive than optical exposure because the writing speed is slow and the system cost is high. Therefore it is only used for making masks or where the high cost can be offset by the savings that result from eliminating the mask. The latter is the case for certain types of custom devices, and in research and development.

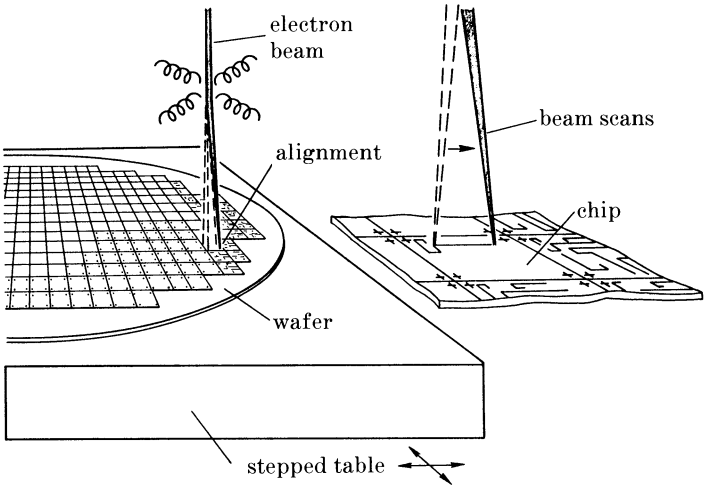

Figure 16. Basic scanning electron beam lithography method.

Electron-beam lithography produces higher resolution than any other method and is therefore best for fabricating nanostructures. So far all structures smaller than 0.1 μm that have been useful as devices have been made with electron-beam lithography.

7.2. *System configurations and throughput*

7.2.1. *Introduction*

As I discussed at the beginning of this lecture, progress in microelectronics has been made by increasing the number of devices on a wafer and, at the same time, holding the cost of the processed wafer constant. Some of this progress has been due to improved device and circuit design, but the greater part has been due to smaller dimensions and larger wafers. The relentless increase in the number of pattern elements on a wafer places greater and greater demands on the inherently serial scanning electron-beam method. Just to keep up in wafer throughput is a formidable task and it appears unlikely that scanning electron beams will do more

than just keep up as wafers of 0.5 μm dimension and 200 mm diameter are introduced.

Throughput of electron-beam systems is limited by the time taken to expose the resist rather than by the overhead times taken to load and position the sample and to deflect the beam. This situation has persisted despite more than two decades of efforts to improve the overall average beam current for given resolution and to develop more sensitive resists. The problem will remain until resists with sensitivities better than about 10^{-7} C cm^{-2} are found because, as discussed later, electron–electron interaction effects limit the maximum current density that can be obtained in the electron beam.

Ultimately, even improving the resist sensitivity will not be useful because the number of electrons required to expose the resist will cease to be large enough to produce a statistically repeatable dose. This will occur, for example, when the resist sensitivity reaches 10^{-7} C cm^{-2} for a pixel size of about 0.1 μm (Everhart 1984).

As with the optical systems, it is not possible with a scanning electron-beam system to cover the whole wafer without moving the sample. This is because of the aberrations of the deflection coil and noise in the electronic deflection signal. Various combinations of mechanical movement and electronic scanning are used to overcome this limitation.

The position of the beam with respect to the sample is maintained in several ways. In the step and repeat systems, a beam to sample reference is made before each section of the pattern (chip) is exposed. The reference is made by collecting scattered electrons as the beam passes across marks on the wafer surface. High-energy electrons are detected rather than low energy secondaries, so that the alignment marks can be detected through resist layers. Position, magnification, rotation, and orthogonality are checked by using at least three marks at each chip site. After registration, the chip is written with a two-dimensional electronic scan. A laser interferometer is also included in many cases to provide an alternative method for keeping track of the sample position.

In the other major type of electron-beam system, the EBES (electron beam exposure system), electron beam mask-maker, the beam is electronically scanned in one direction only and the sample moved continuously in the orthogonal direction (Herriot *et al.* 1975; Alles *et al.* 1987). Chips are written strip by strip, the same strip on every chip being written before proceeding to the next strip. The position of the beam is checked initially with a direct beam to sample measurement, and then a laser interferometer keeps track of the sample. Errors in the relative position of the beam and the sample are corrected by feeding signals to the electron-beam deflection coils.

With either method, the ability of electrons to penetrate the resist and 'see' the alignment marks is a key attribute of electron lithography.

7.2.2. *Shaped beam against round beam?*

Three basic methods have been used to maximize electron-beam current and minimize writing time. The first uses a rectangular beam the size of which is changed to fill the pattern features (Pfeiffer 1978; Goto *et al.* 1978; Thomson *et al.*

1978). This variable-shaped spot (vss) minimizes the number of beam addresses and maximizes beam current for a given beam current density. The second uses beams of different sizes, for example a small round beam for outlining shapes and a large round or square beam for filling in the centres of the shapes. The third uses a small round beam alone. Here the beam, which is about four times smaller than the minimum feature size, 'paints in' the pattern elements (Chang *et al.* 1976; Varnell *et al.* 1979). Full pattern flexibility is retained in this last case, that is the ability to write curved and angled lines, but the average current is not as high as it is in the other two cases, although as discussed later, somewhat higher current density can be obtained than in the vss case. The number of beam addresses is smallest with the vss approach.

Variable shaped beams are formed by superimposing the image of one square aperture onto a second square aperture (see figure 17). Non-square apertures have also been used to produce non-rectangular shapes. The shape of the final beam

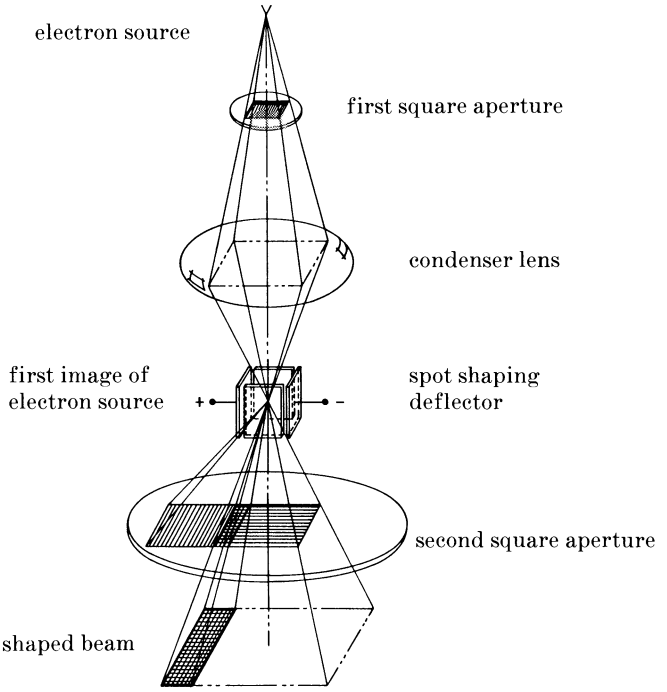

FIGURE 17. Method for forming variably shaped spot (vss) electron beams for lithography (Pfeiffer 1978).

depends on the position of the image of the first aperture on the second aperture. Both Koehler and critical methods have been used to illuminate the first shaped aperture. In general, Koehler is preferred because it allows the electron-beam column to be shorter.

Recently Koehler and critical illumination have been combined in a method in which the focusing action of the gun electrodes images the cathode surface on to the shaped aperture, and simultaneously the condenser lens images the cross-over

formed in the gun on to the entrance pupil of the final lens. This improves uniformity of illumination at the shaped aperture and should allow the current density to be increased (Essing & Pfeiffer 1986).

Provided that the electron gun produces adequate current at a given brightness, the brightness in a shaped beam is the same as that in a round beam, in fact, the average brightness is higher if the round spot has a gaussian current distribution. This means that for the same beam aperture and beam brightness, the beam current in the shaped beam is higher by at least the ratio of the spot areas.

The larger the shaped spot, the larger the beam current, and the smaller the number of beam addresses. This approach cannot be taken too far, however, because as the current increases, electron–electron interactions increase and edge definition degrades because of the increased energy spread in the beam. For example, in the EL3 system, which has a beam current density of 50 A cm^{-2} and a maximum spot size of 4 μm × 4 μm (16 $μm^2$), spot edge definition degrades beyond 0.25 μm for spots larger than about 6 $μm^2$ (Pfeiffer 1979). Larger spots could be used if the current density was reduced but this would increase the exposure time for the majority of shapes, which are generally smaller than 6 $μm^2$. The optimum spot size is that which maximizes the average beam current over the writing time. To minimize exposure time, the current density is kept relatively high, and the problem of poor edge definition on large shapes is overcome by outlining these shapes with small narrow rectangles. In principle, it is also possible to modulate the brightness according to the beam size but to date this has not been thought to be worthwhile.

For the current in a round beam to equal that in a shaped beam, the spot current density must exceed that in the shaped beam by the average number of resolution elements projected in the shaped beam. The average number of resolution elements is typically 30–100, or about 2–6 minimum feature size squares. As already discussed, the current in the shaped beam is limited by electron–electron interactions and for example, this limit is reached in EL3 at a gun brightness of about 3×10^5 A/ cm^{-2} sr (25 kV). So to obtain comparable current with a single round beam, a brightness of 1×10^7–3×10^7 A cm^{-2} sr^{-1} would be needed.

Such brightness is available from field emitters and thermal-field emitters, but only at relatively small final-beam currents (less than 1 μA). At about 10 μA, which is the current produced in a vss system for 1 μm linewidth lithography, the beam aperture must be increased to the point that the aberrations of the electron lens formed by the gun accelerating electrodes degrade the brightness by increasing the effective source size. The brightness can be maintained at higher currents by increasing the total current drawn from the source, but this degrades stability.

Lanthanum hexaboride cathodes fall short of the required brightness for a round beam to compete with a shaped beam only producing about 1×10^6 A cm^{-2} sr^{-1} (25 kV) with adequate reliability for production applications (Broers 1975). Figure 18 shows brightness against total current drawn from the source for thermal and thermal-field-emission sources. It is clear that brightness of 10^7 A cm^{-2} sr^{-1} is not available for final beam currents of 10 μA. The example of an ion source shown in figure 18, is discussed later.

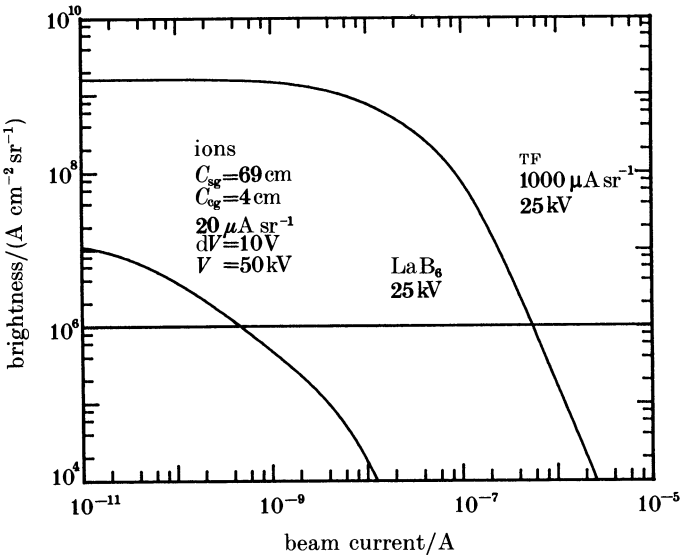

FIGURE 18. Brightness against total current drawn from the source for a lanthanum hexaboride thermal-electron source, a thermal-field-emission source (TF emitter), and a liquid ion source.

In summary, it is not possible with presently available sources to obtain the same thoughput with a round beam as with a shaped beam. The case where round beams of different sizes are used falls between the two other cases.

7.2.3. *Round-beam vectorscan systems*

In vectorscan systems the beam is directed only to those areas of the chip that require exposure. As already mentioned, the beam diameter with a round beam is equal to one quarter of the minimum linewidth. This means that the beam must be incremented to sixteen positions to write a single minimum image square. Chip writing time can be estimated from the beam incrementing rate, and the average fraction of the chip area than needs to be exposed. For example, with a 1 μm image, a 5 mm × 5 mm chip contains a total of 25×10^6 minimum images, of $16 \times 25 \times 10^6$ beam positions. If, on average, 25 % of the chip is exposed, then 10^8 beam positions must be written per chip. At 20 MHz, which is the maximum rate used so far to make integrated circuits (higher rates have been reported for systems while in their development phase but this level of performance has not been sustained in final implementation), this will take 5 s. The 50 ns taken to expose each pattern element includes both the electronic settling time and the resist exposure time. Time taken for table stepping, registration, wafer loading, and data transfer is added to the writing time to arrive at the overall time per wafer shown in tables 2 and 3 and figures 19 and 20.

7.2.4. EBES; *continuously-moving table; rasterscan; round beam, systems*

The EBES system uses a small round electron beam that is deflected to every element on the wafer whether or not exposure is required (advanced EBES systems skip kerf areas and areas where no exposure is required but still write the rest of

the areas in a raster manner). If the grid on which the pattern is written is finer than the beam diameter, as is typically so for masks where the ratio of minimum image to design grid can be as high as 20 : 1, then the number of beam addresses becomes greater than would be expected from the beam diameter. This means that the throughput of an EBES system scales inversely with the square of the image design grid.

7.2.5. EL3; *variable-shaped beam; subfield deflection; vectorscan system*

EL3 combines a high-current variable-shaped beam column with a dual deflection system and a high-speed laser interferometrically controlled sample stage (Moore *et al.* 1981). For an EL3 designed for 1 μm linewidth, beam shapes up to a maximum of 4 μm × 4 μm are available in 0.1 μm increments. Spot-edge definition is better than 0.2 μm. The dual deflection system consists of a highly accurate but relatively slow magnetic deflection that deflects the beam in a raster sequence to the centre of an array of 75 μm × 75 μm subfields and a higher-speed but lower-accuracy electrostatic deflection that vector-addresses the shaped beam inside the subfields. The subfields are overlapped to avoid discontinuities and the array of subfields can be as large a 10 mm × 10 mm.

Positional errors in both magnetic and electrostatic deflection are measured by scanning a reference grid. These errors are stored in the control computer and corrections fedback during writing. This procedure is needed to achieve accuracy both in joining the subfields and in layer to layer overlay.

It is possible with most electron-beam lithography systems to scale down the operating parameters and produce smaller dimensions. In general, the field size has to be reduced in proportion to the minimum feature size and the throughput is reduced as the square of the minimum feature size. Versions of EL3 have been built for linewidths of 0.5 μm and below by using such scaling. A version of EL3 for mask-making has also been described (Hsia & Weber 1985).

7.2.6. AEBLE; *variable-shaped beam; continuously moving table; vectorscan system*

In principle, highest throughput in scanning electron beam lithography is obtained with a continuously moving table and 'on-the-fly' registration and writing. In the AEBLE system this idea is combined with the use of a variable shaped beam. The shaped beam is vector-addressed to write the pattern and the speed of the table is varied according to the pattern density. To accomplish the latter, the control computer looks ahead and determines the density of the pattern that is about to be written. In practice, the time taken to step and register the beam is small compared with the writing time, or even to the pattern-generator electronic switching and settling times, and the advantage of 'on-the-fly' operation is small. As a result, the throughput of AEBLE when it is in full operation may be no higher than that of EL3. Early work leading to the development of AEBLE has been described by King *et al.* (1985).

7.2.7. *Throughput summary*

Tables 2 and 3 and figures 19 and 20 compare the throughput of different electron beam systems for combinations of 150 mm wafers and 1 μm dimensions (present), and 200 mm wafers and 0.5 μm dimensions (future). The vectorscan

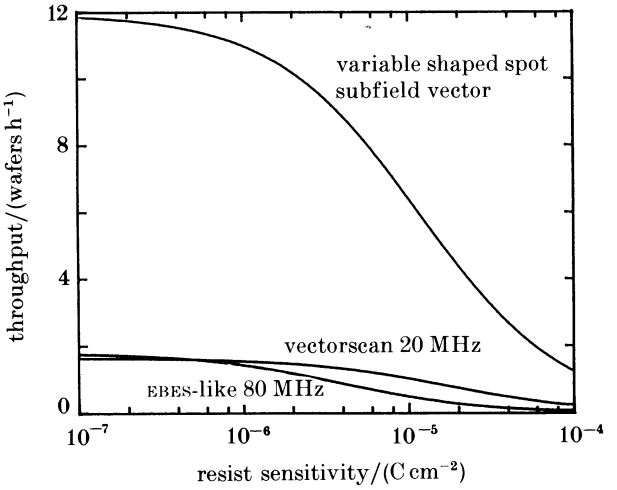

FIGURE 19. Throughput of 125 mm wafers against resist sensitivity for 'present' electron beam lithography systems. Pixel size is 0.25 μm.

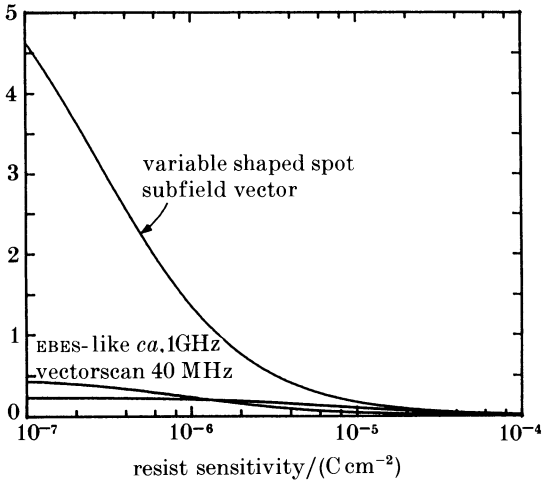

FIGURE 20. Throughput of 200 mm wafers against resist sensitivity for 'future' (*ca.* 1990) electron beam lithography systems. Pixel size is 0.1 μm.

system is assumed to use pure electronic scanning with a single deflection coil. The present variable shaped spot system is assumed to use subfield electronic scanning of the type used in EL3 and the future VSS to use a combination of a variable speed table and electronic vector scanning as used in AEBLE. EBES-like systems are assumed to use a combination of a line-scan and continuous mechanical movement.

Most of the parameters are self-explanatory except for the following.

Pixel-rate. The equivalent incrementing rate of a round-beam vector-scan system. For example a raster scan system such as EBES is only considered to have an incrementing rate of the beam address rate multiplied by the fraction of the area that has to be exposed. This yields a lower rate than is normally quoted.

TABLE 2. THROUGHPUT FOR PRESENT ELECTRON-BEAM LITHOGRAPHY SYSTEMS

	vss	vector scan, 20 MHz	EBES-like, 80 MHz
pixel size/μm	0.25	0.25	0.25
spot current density/(A cm^{-2})	50	300	300
resist sensitivity/(C cm^{-2})	10^{-5}	10^{-5}	10^{-5}
pixels per shape	30	1	1
pixels per subfield	400×400	—	—
chip size/mm	5	5	5
wafer size/mm	125	125	125
percentage exposed	25	25	100
subfield to subfield time/μs	20	0	0
shape to shape time/ns	50	50	12.5
chip to chip time/s	0.5	0.5	0
125 mm wafer throughput/h^{-1}	6.4	1	0.5

TABLE 3. THROUGHPUT FOR FUTURE ELECTRON BEAM LITHOGRAPHY SYSTEMS

	vss continuous table	vss continuous, short focal length lens	EBES-like, ~ 1 GHz
pixel size/μm	0.1	0.1	0.1
spot current density/(A cm^{-2})	20	200	300
resist sensitivity/(C cm^{-2})	3×10^{-7}	3×10^{-7}	3×10^{-7}
pixels per shape	30	30	1
pixels per subfield	$10^3 \times 10^3$	$10^3 \times 10^3$	—
chip size/mm	20	20	20
wafer size/mm	200	200	200
percentage exposed	25	25	100
subfield to subfield time/μs	10	10	0
shape to shape time/ns	5	5	1
chip to chip time/s	0	0	0
200 mm wafer throughput/h^{-1}	8	20	0.7

Pixels per shape. The average number of pixels (resolution elements) exposed for each beam flash. The value of 100 used in these calculations for the vss system is, for example, equivalent to an average beam area of about 6 μm^2 for edge definition of 0.25 μm.

Pixels per subfield. The number of pixels in the subfield of the dual-level deflection assumed for the vss system. This number determines how many subfield to subfield delay times have to be added to the chip exposure time.

Subfield to subfield time. The settling time of the magnetic deflection system that deflects the beam between subfields (only incurred for the dual-level vss deflection systems).

Shape-to-shape time. The settling time of the high-speed deflection that deflects the beam from shape to shape. The vectorscan and the vss are assumed to be the same. This is probably optimistic for the vectorscan case because the vectorscan

deflection has to cover the whole field rather than just a subfield. The shape-to-shape time for the EBES raster system is assumed to be considerably shorter than that for the vector systems because of the repetitive nature of the raster deflection.

Spot current density. Current density in the shaped beam is assumed to be lower than with the small round beams because of electron–electron interactions. It is also assumed that the current density is the same for the EBES as for the vectorscan which has not been so for most of the earlier EBES systems which have had lower current density.

7.3. *Future systems: short-focal-length lens*

One way to increase current density, without increasing energy spread, is to use a final lens with very short focal length similar to those used in transmission electron microscopes (Broers & Coane 1986). These lenses have much lower on-axis aberrations than the lenses normally used in electron beam fabrication systems and would, through the use of larger apertures and therefore without increasing electron–electron interactions, allow up to 20 times higher current density. The deflection field would have to be very small, but a combination of mechanical movement and electronic deflection could be used to cover large samples. The sample would be immersed in the magnetic field of the lens, as has already been done with the VAIL concept (Kern *et al.* 1984), and with a high-resolution system built for nanolithography by Newman *et al.* (1987). The performance of a system with a short-focal-length lens is shown in table 3.

Another method that has been proposed for increasing the beam current for a given spot size is to form the beam from a series of 'beamlets' that are separated for much of their path in the electron optical column thereby minimizing electron–electron interactions (Van der Mast *et al.* 1985). This 'shower beam' idea, which is yet to be implemented in a full lithography system, offers the potential for a tenfold increase in current density.

Although it is theoretically possible through the use of short-focal-length lenses or shower beams in combination with a resist sensitivity of 10^{-7} C cm^{-2} to reach the throughput of either optical projection cameras or storage-ring X-ray lithography, it is unlikely that this will be accomplished within the foreseeable future because of the accompanying advances that would have to be made in the performance of the deflection and data control systems.

7.4. *Proximity effect*

Proximity effect is the name given to the effect in electron-beam lithography that makes exposure at one point depend on whether or not surrounding points are exposed (Chang 1975). It arises because electrons are back-scattered from the substrate beneath the resist into regions surrounding the point of impact of the beam. Figures 21 and 22 show qualitatively the exposure distributions and physical mechanisms for proximity effect. It can be seen that the area exposed by the back-scattered electrons depends strongly on the energy of the incident electrons. For higher electron energies (more than 25 keV), the exposure due to back-scattered electrons is spread over a relatively large area and tends to reduce image contrast rather than to affect resolution.

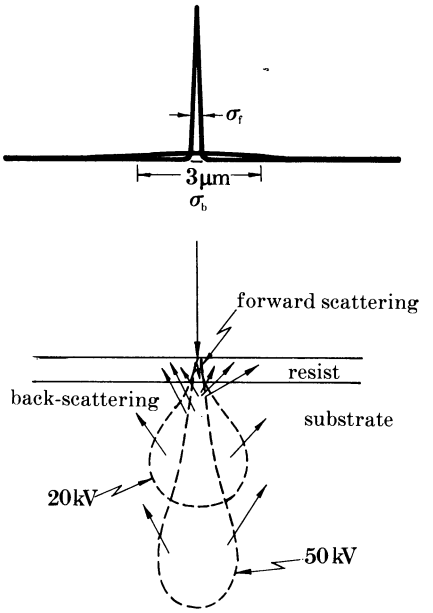

FIGURE 21. Physical mechanisms of electron-beam proximity effect. σ_f, Forward-scattering distribution; σ_b, back-scattered distribution (20 kV). Proximity function $f_p(r) = k[\exp(-r^2/\sigma_f^2) + \epsilon(\sigma_f^2/\sigma_b^2)\exp(-r^2/\sigma_\beta^2)]$.

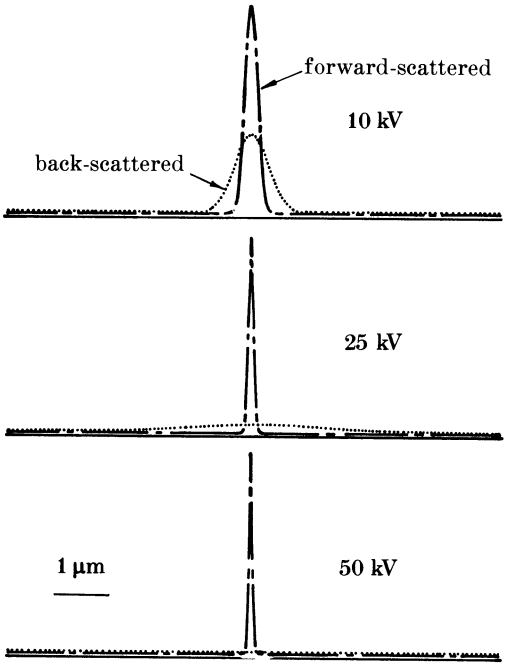

FIGURE 22. Approximate exposure distributions for exposure with 10 kV, 25 kV and 50 kV electrons.

Proximity effect gives rise to differences of up to 60% between the exposure dose at the centres of large and small shapes. Smaller differences arise due to the number and proximity of neighbourhood shapes. If the resist process is such that the differences produce unacceptable variations in the developed size of shapes then it is necessary to vary the dose for each shape. For a complex integrated circuit pattern, the calculation required to determine the individual doses is very large and computing expense becomes a significant factor in deciding whether or not to use scanning electron beam lithography for a given application. Perfect compensation for proximity effect is not possible because negative exposure dose would be required.

Proximity effect can be minimized, at the expense of process complexity, by using multilayer resists. To ensure high contrast and high resolution, the upper layer in which the image is formed is kept thin, and the underlayer thick. The thick underlayer backscatters fewer electrons than a typical substrate because it has lower atomic mass.

7.5. *Resolution and nanolithography*

7.5.1. *Introduction*

The resolution of electron beam resist exposure is set by three factors.

1. Scattering of the primary electrons as they penetrate the resist. This form of scattering, which is usually called 'forward-scattering', can be made to be negligible through the use of high accelerating voltages (more than 50 kV) and thin resist layers (less than 0.1 μm). It is not important in setting the ultimate resolution limit.

2. Back-scattering of electrons from the substrate underneath the resist. The diameter of the disc from which these backscattered electrons energy depends on the electron energy and, for accelerating voltages of more than 50 kV, is greater than 5 μm. For linewidths below 1 μm, therefore, back-scattered electrons only reduce contrast resolution by reducing. This is discussed further in the next section. For small isolated features, back-scattered electrons have negligible effect on resolution.

3. A combination of the range of the interactions between the electrons and the resist molecules, and the distance travelled by the low-energy secondary electrons created by these interactions. This is the primary factor setting the ultimate resolution.

It is always possible, if exposure speed is not important, to keep the beam smaller than these other effects. Ultimately, the minimum dimensions in resist are about 10 nm, whereas beam diameters can be as small as 0.3 nm. The 10 nm limit is thought to occur because exposure is largely due to secondary electrons, and secondaries are generated up to 2 nm from the primaries, and can straggle several nanometres further into the resist before their energy is dissipated.

Figure 23 shows the relation between beam diameter and beam current for electron- and ion-beam systems suitable for fabricating devices with dimensions between 0.1 and 1 μm. The method used to calculate these relations has been described in Broers (1972). The ion-beam example is discussed later. Figure 24 shows the case for the LaB_6 cathode electron-beam system used to fabricate the

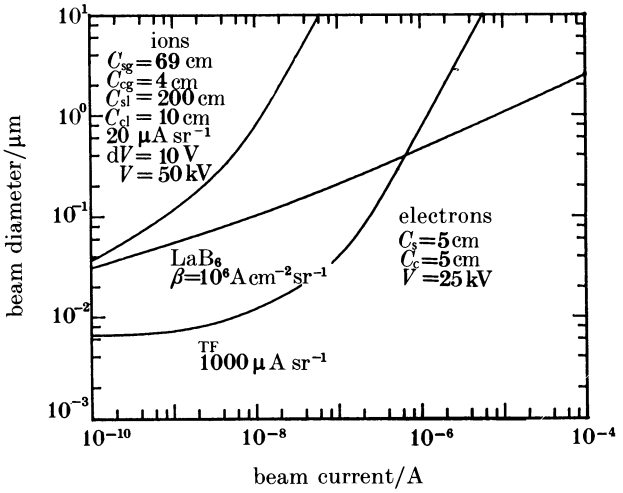

FIGURE 23. Beam size against beam diameter for electron-beam and ion-beam systems suitable for fabricating devices with dimensions between 0.1 and 1 μm. Aberration, current density and, brightness data for these estimates are given by Broers (1972).

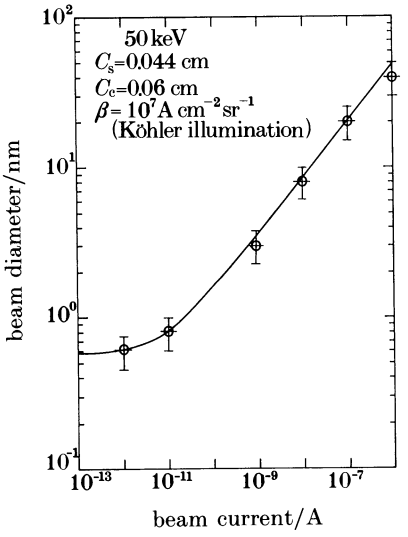

FIGURE 24. Beam size against current for LaB_6 cathode electron-beam system used to fabricate all the nanostructure devices and exposures shown in this paper.

nanostructure devices shown in this lecture. Currents down to about a picoamp were used for nanolithography.

Figure 25 shows methods for fabricating nanostructure devices with conventional resists.

7.5.2. *Ultimate resolution in resists*

It is difficult to measure the ultimate resolution of electron-beam resist exposure because the electron microscopes needed to make the measurements distort the

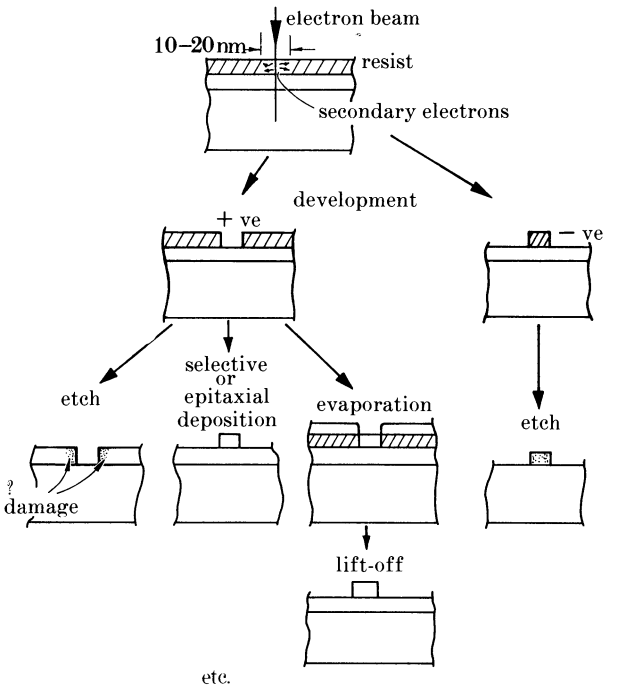

FIGURE 25. Methods for using conventional resists for the fabrication of nanostructures.

resist test patterns. This has led to the development of a method that determines the effective exposure distribution without the need to measure linewidth (Broers 1981). All that is required is a knowledge of the 'written' linewidth, which is set by the electron-beam pattern generator, and a determination of which lines are completely exposed at each exposure dose. Having measured the exposure distribution, it can than be used to evaluate resolution in the same way the Airy distribution is used to determine the resolution of a diffraction-limited optical microscope.

A test pattern of the type used to determine the exposure distribution is shown in figure 26, plate 1. The pattern was written in a 60 nm thick layer of PMMA with a 50 kV electron beam, whose diameter was less than 1 nm. The minimum linewidth is about a factor of three smaller than the half-width of the distribution, and the largest linewidth is about 10 times greater than the half-width. For each experiment, the pattern is repeated at about 10 different exposure doses. The lightest dose is below that needed to open up the largest shapes. The heaviest dose is high enough to ensure that the resist develops through to the substrate in the site of the narrowest line. The exposure in figure 26 is slightly above that needed to open up the largest shapes.

If it is assumed that the exposure distribution is guassian, and that the lines are equivalent to infinitely long rectangles, then the exposure dose, Q_W, in coulombs per square centimetre received at the centre of a line given by

$$Q_W = Q_0 \operatorname{erf}(W/2\sigma),$$

where Q_0 is the exposure dose in the centre of an infinitely large shape in coulombs per square centimetre, and σ is the standard deviation of the distribution. Q_W is measured for each linewidth by determining the dose at which the line first develops through to the substrate. As the exposure increases, narrower and narrower lines develop through to the substrate. The exposure distribution is calculated from the Q_W against linewidth data.

Figure 27 shows data obtained with PMMA of different molecular masses showing that there is little or no dependence on molecular mass, thus removing the possibility that it is the molecular mass that sets the 10–20 nm measured resolution limit. These experiments, which are reported here for the first time, were carried out in collaboration with C. G. Willson, C. Umbach and R. Laibowitz.

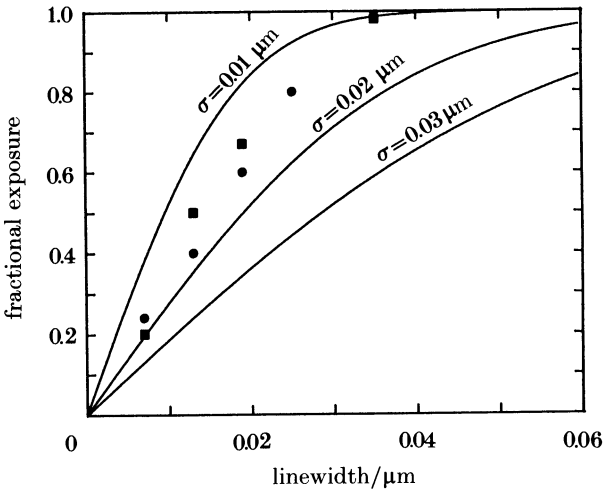

FIGURE 27. Fractional exposure data for PMMA of 20000 (■) and 500000 (●) molecular mass. The difference between the data for the different molecular masses is negligible suggesting that there is no dependence on the molecular mass of the sample. These experiments were carried out in collaboration with C. G. Willson, C. Umbach and R. Laibowitz.

The measurements of resist resolution just described are made on the thin thin-film substrate shown in figure 28 which was developed for the fabrication of structures with dimensions less than 0.1 μm (Sedgwick *et al.* 1972; Broers & Sedgwick 1976). The substrate allows samples to be examined and written upon in a transmission electron microscope (scanning or projection), as in the evaluation of resist resolution, and also makes it possible to make electrical contact to the structures on the fragile membrane. This is done by the leads that extend out from the bulk area. Thin membranes of a variety of materials have been made and it is possible, for example with silicon or GaAs membranes, to fabricate devices using the membrane as part of the device.

In figure 29 the data for the thin substrate are combined with data for the backscattering distribution from bulk substrates to come up with an overall estimate of the resolution of electron beam exposure of PMMA on bulk and thin substrates. The exposure value plotted is that obtained at the centre of square apertures. The forward and backward exposure distributions are assumed to be

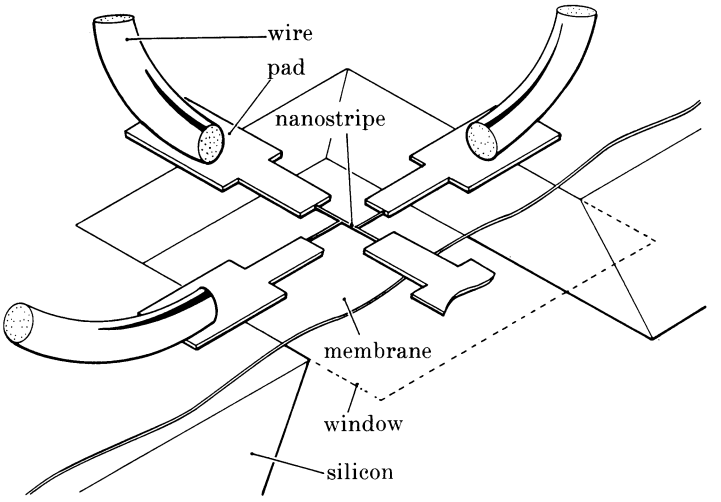

FIGURE 28. Thin membrane substrate used for the fabrication of nanostructures (Sedgwick *et al.* 1972; Broers & Sedgwick 1976).

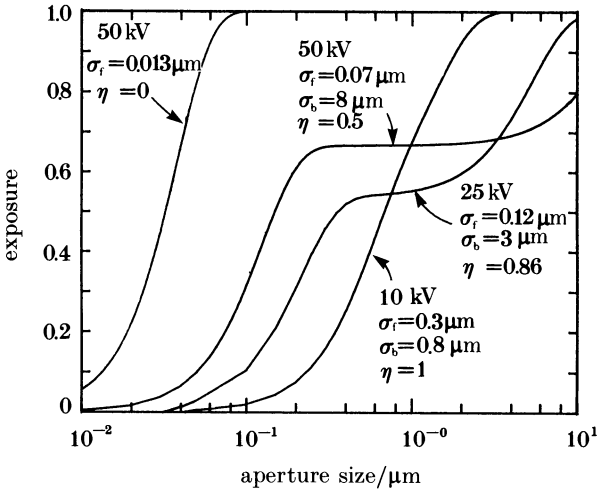

FIGURE 29. Normalized aperture exposure (ratio of the exposure received at the centre of a square aperture of a given size to the nominal background exposure) for 10 kV, 25 kV and 50 kV electron beam exposure of a 1 μm thick PMMA resist layer on a silicon substrate. The case for thin resist and a thin substrate is also shown; – σ_f is set by the secondary electron interaction range.

gaussian and the expression for the overall exposure is that given in figure 21. The forward-scattering sigmas are those obtained in a recent set of experiments in which the exposure distributions in 1 μm thick PMMA layers were measured in a similar manner to that described above for the measurement of ultimate resolution. It can be seen from figure 29 that backscattering reduces contrast but does not change the ultimate resolution very much. In practice a contrast of 50% is adequate for the fabrication of high-quality structures, so minimum dimensions approaching 10 nm are possible with the thin substrate.

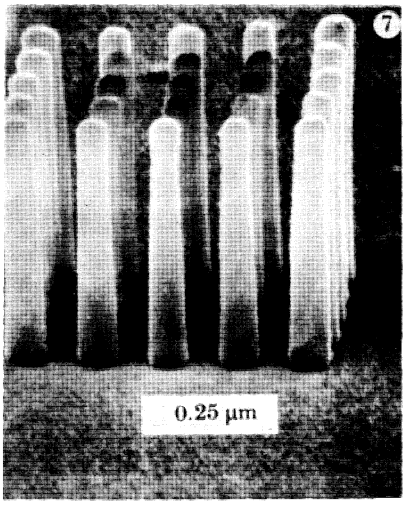

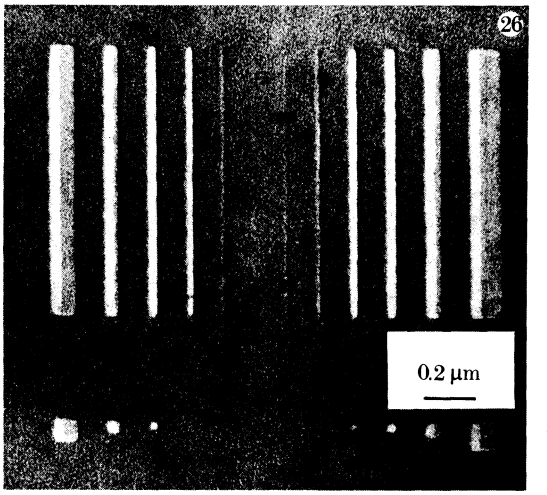

FIGURE 7. High-aspect-ratio resist patterns fabricated with X-ray lithography (Heuberger 1987*b*).

FIGURE 26. One of a series of test patterns used to measure the resolution of electron resist (Broers 1981). The 60 nm thick PMMA resist layer is supported on a 60 nm thick Si_3N_4 membrane and the pattern has been exposed with a 0.5 nm diameter 50 kV electron beam. The sample has been shadowed at 45° with AuPd to highlight the structure and to reveal the resist thickness. This particular exposure is made at a slightly larger dose than is needed to open up the largest shapes in the pattern.

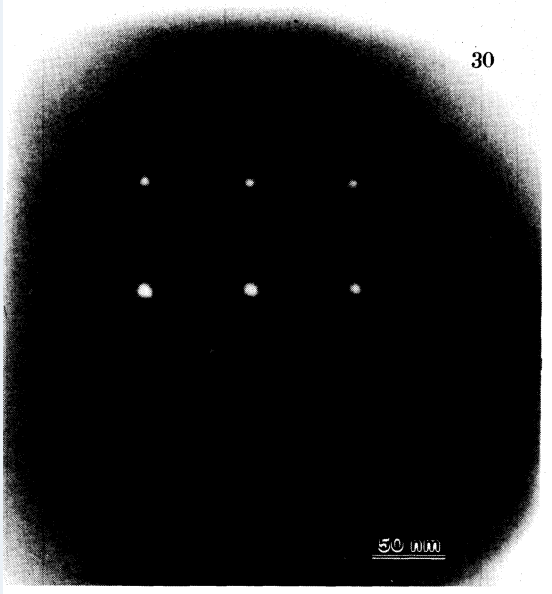

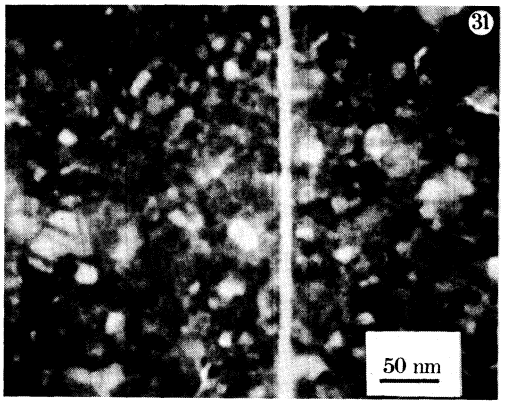

FIGURE 30. 5 nm diameter holes drilled in NaCl with 1 nm diameter electron beam (Broers *et al.* 1978).

FIGURE 31. A 10 nm wide slot ion milled in a 20 nm thick gold film using directly patterned MgF_2 as a mask.

(*Facing p.* 32)

PROCEEDINGS OF THE ROYAL SOCIETY A MATHEMATICAL, PHYSICAL & ENGINEERING SCIENCES

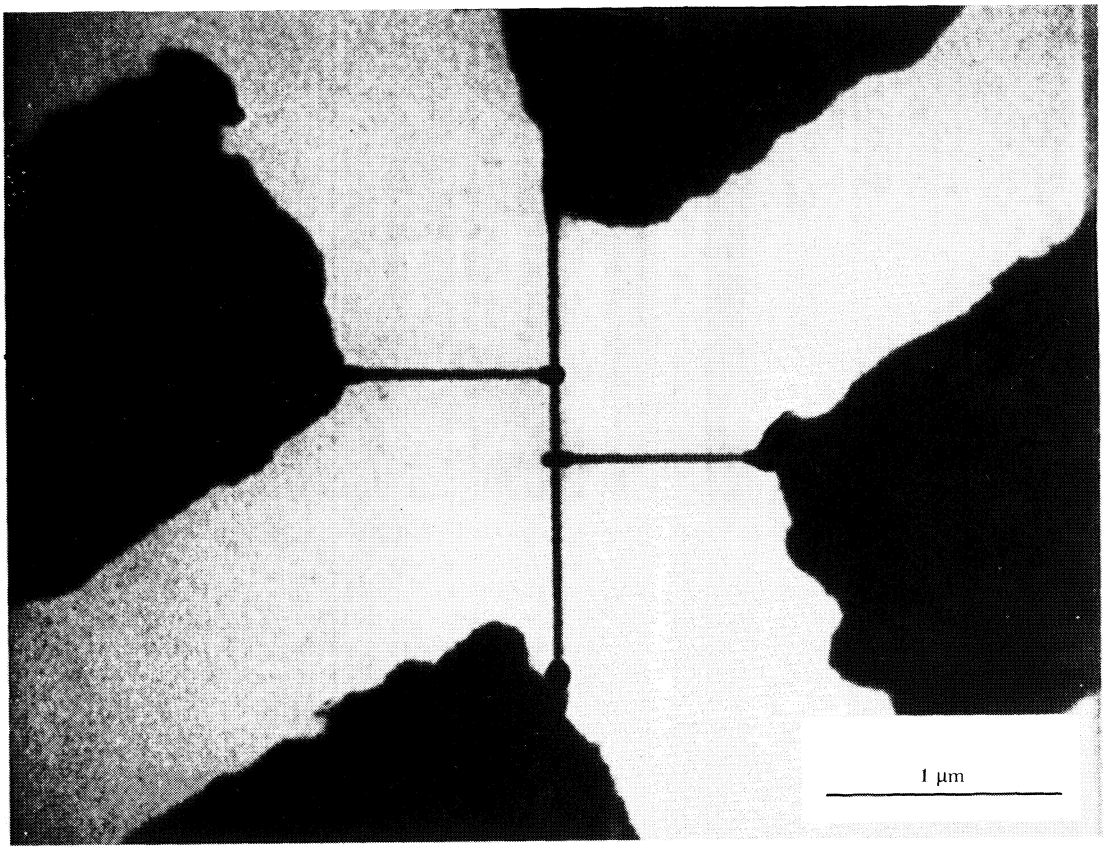

FIGURE 36. 25 nm wide niobium wires in a four-terminal configuration used for exploring localization effects (Laibowitz *et al.* 1979).

PROCEEDINGS OF THE ROYAL SOCIETY A MATHEMATICAL, PHYSICAL & ENGINEERING SCIENCES

7.5.3. *Structure fabrication for dimensions below* 10 nm

(*a*) *Direct sublimation*. To avoid the 10 nm limit encountered with conventional electron resists such as PMMA, it is necessary to find an image-forming process that is activated only by the high-energy primary electrons, and not by the low-energy secondaries.

One process which appears to behave in this manner is the direct sublimation under electron bombardment of a variety of materials including NaCl, MgF_2, AlF_3, LiF and Al_2O_3. The high resolution of this process was discovered in the experiments proposed by J. W. Matthews that produced the 5 nm diameter holes shown in figure 30, plate 1. The holes were formed in a NaCl crystal by a 1 nm diameter 50 kV electron beam (Broers *et al.* 1978, 1981). The crystal was 0.25 μm thick. The convergence half-angle of the beam was 10^{-2} rad, and assuming that the beam is focused on one face of the crystal, the beam would have formed a conical hole with the base of the cone being about 5 nm in diameter. This would explain the difference between the apparent size of the hole and the beam diameter, and suggest that the resolution of the process was better than 5 nm. These experiments were continued to show that it was possible to use a patterned MgF_2 film to mask a gold film from ion milling and to produce slots less than 10 nm in width in a 20 nm thick gold film (see figure 31, plate 1). In general, however, the films did not stand up well to a variety of dry or wet etching techniques.

Isaacson & Muray (1981) confirmed that resolution below 5 nm is possible with direct sublimation by writing structures down to 1.5 nm in size in thin NaCl and AlF_3 films. Kratschmer & Isaacson (1986) used one of the patterned AlF_3 films to mask a silicon nitride film against dry etching but the smallest structures produced in the nitride were about 20 nm in size.

Mochel *et al.* discovered that the sublimation process works with Al_2O_3 and produced holes 1 nm in diameter (Mochel *et al.* 1983). Both Mochel *et al.* and Isaacson *et al.* have used EELS (electron energy loss spectroscopy) to analyse the process and have shown that, in general, a metal-rich deposit remains after the sublimation process. The details of the sublimation mechanism remain unclear, however, and it has yet to be shown that the process can produce devices of practical importance.

Some of the ways in which device structures might be made with direct sublimation lithography are shown in figure 32.

(*b*) *Radiation-damage lithography*. It may be possible to fabricate structures smaller than the secondary electron range through a new class of processes which use electrons whose energy is great enough to introduce radiation damage in the sample. For crystalline materials such as silicon this requires an energy above about 150 kV. Several possible methods for coverting the damaged areas into structure are shown in figure 33. The damage may enhance or retard the etch rate of the material for dry or wet etch processes, it may locally change other properties such as the critical temperature for superconductors, or it may locally affect the integrity of epitaxial films grown on the substrate. For epitaxial films, damaged areas may etch at different rates to defect-free areas or exhibit different

PROCEEDINGS OF THE ROYAL SOCIETY A MATHEMATICAL, PHYSICAL & ENGINEERING SCIENCES

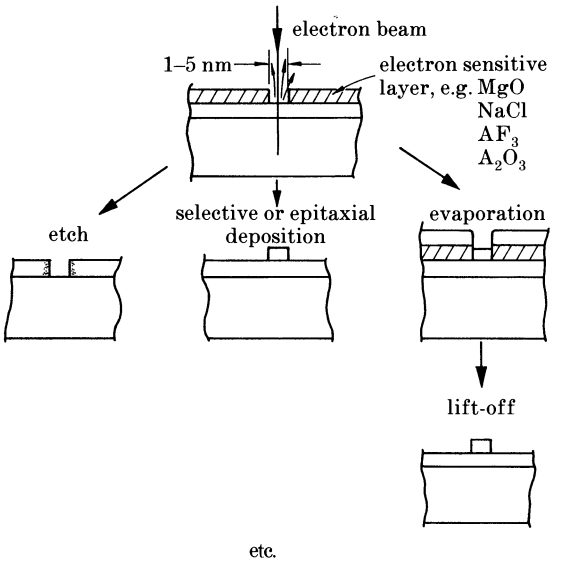

FIGURE 32. Possible methods for fabricating structures with direct sublimation electron-beam lithography. Selective deposition methods could include electroplating.

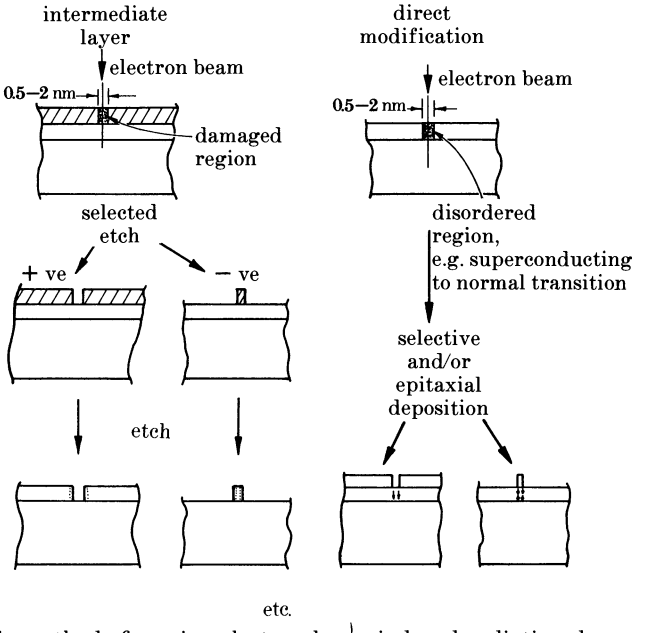

FIGURE 33. Possible methods for using electron-beam induced radiation damage lithography to fabricate structures.

electrical properties (conductivity, etc.). An example of the latter might be that regions of a superconducting film deposited on damaged areas of a single crystal substrate would exhibit normal conductivity and therefore act as weak links between the superconducting regions grown on the undamaged areas.

Electrons with an energy of less than half the damage threshold energy would

be used for radiation damage lithography so that only a single damage event would be created by each electron. The damage should then be localized within the beam diameter which can be as small as 0.3 nm. Jones *et al.* (1986) have done some preliminary low-resolution experiments to explore these methods and we are building in the Cambridge University Engineering Department a high-voltage electron probe with a diameter below 0.5 nm to investigate the high-resolution possibilities of the processes.

7.6. *Nanostructure devices*

The first useful nanostructures were fabricated in the early 1970s with PMMA resist and the lift-off process (Mayadas & Laibowitz 1972). They were aluminium wires with cross sections of about 60 nm × 60 nm which were used to measure excess fluctuation conductivity over a temperature range much larger than had previously been possible. Structures of similar size had been made in the early 1960s but they were not used for any purpose, they were merely examined in an electron microscope (Mollenstedt & Speidel 1960; Broers 1965*a*, *b*).

Following the aluminium wires, a variety of nanostructure devices were made with 'contamination resist' and ion etching. The contamination resist process had been developed in the early 1960s but the first useful devices were not made until 1978 (Broers & Laibowitz 1978). Contamination resist is formed from the thin layer of hydrocarbons that condenses onto a sample when it is placed in a vacuum system in which there is a high partial pressure of hydrocarbons (see figure 34). The electron beam 'cracks' the hydrocarbons at the sample surface and a cone of resist builds up at the point of impact of the electron beam. Under certain conditions, the rate of build-up can be increased by increasing the partial pressure

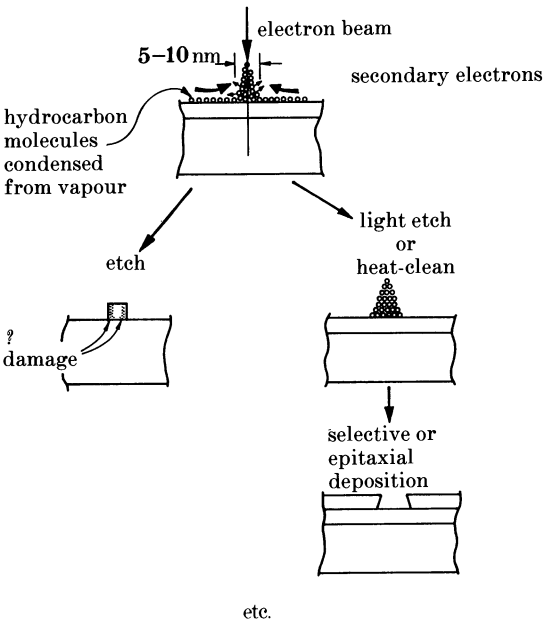

FIGURE 34. Vapour resist (contamination) method for producing high-resolution electron-beam lithography (Broers 1965*a*, 1965*b*).

PROCEEDINGS OF THE ROYAL SOCIETY A MATHEMATICAL, PHYSICAL & ENGINEERING SCIENCES

of hydrocarbons in the immediate vicinity of the sample with a local source of vapour. A dose of 0.1–1 C cm^{-2} is required to produce an adequate resist thickness for protecting 100 nm thick metal layers (e.g. gold and niobium) from ion etching. This high dose makes it difficult to fabricate large area devices, but has the advantage that the sample can be microscopically examined before and after examination, without significant additional resist build-up. When a substrate of the type shown in figure 28 is used, transmission electron microscopy can be used to position the structures with respect to contact pads, or other device layers, and to examine the resist pattern after it has been formed. The build-up of resist can also be accurately monitored by observing the decay in the transmitted signal.

It is possible to remove the layer of hydrocarbons and stop the build-up of contamination by heating the sample to about 100 °C. Heating can be carried out, for example, with a high-intensity lamp. Removal of the hydrocarbons allows the sample to be examined without further build-up of resist, provided of course that the partial pressure of hydrocarbons is low enough to prevent a new layer of hydrocarbon from being deposited on the surface. It also opens up the possibility for *in situ* fabrication sequences where the vapours which form the resist are selectively introduced when the resist pattern is to be formed and then the surface contaminants removed before, for example, the next thin-film deposition step.

A variety of devices has been made with the combination of contamination resist and ion etching including microbridges (Laibowitz *et al.* 1979), SQUIDs (Voss *et al.* 1980) (superconducting quantum interference devices) as shown in figure 35,

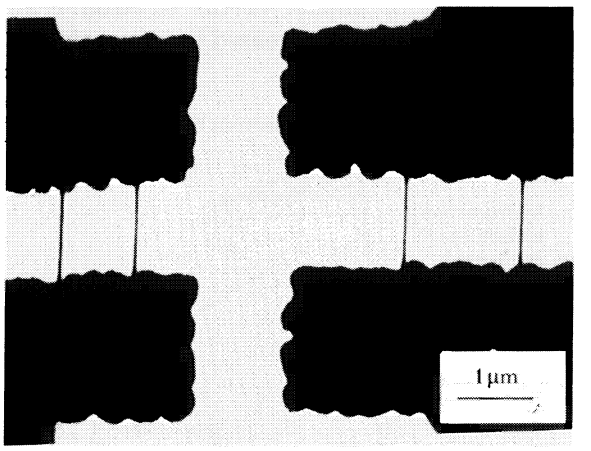

FIGURE 35. Microbridge SQUIDs fabricated with contamination resist electron beam lithography (Voss *et al.* 1980).

fine wires for exploring localization effects (Chaudhari *et al.* 1980) as shown in figure 36, plate 2, and wire rings for demonstrating aspects of the Aharonov–Bohm effect. Buckley *et al.* (1985) have produced high-resolution X-ray zone-plate lenses with contamination lithography.

Recently semiconductor devices with dimensions approaching the nano-structure region have been fabricated with double-layer PMMA based resists and lift-off metalization (Howard *et al.* 1985; Mackie *et al.* 1985).

8. Scanning ion beam lithography

8.1. *Introduction*

Focused ion beams can be used to expose resist, to write diffusion patterns directly into semiconductor substrates, and to repair masks. These techniques can potentially simplify microfabrication processes and perhaps reduce cost. Many of the technological challenges with ion beams are similar to those encountered with electron beams, but the performance of ion optical systems (beam diameter and field size for a given beam current) is poorer than it is for equivalent electron optical systems. This means that at present it does not seem feasible to build an economical scanning ion beam system for integrated circuit fabrication, nor to obtain high enough resolution for nanolithography. On the other hand, ion-beams can be used to modify materials in ways not possible with electron beams and their unique capabilities may prove valuable in a variety of applications.

8.2. *Ion-beam resist exposure*

Ion-beam exposure of resist is free of the deleterious long-range proximity effects of electron-beam exposure. Ions dissipate their energy by introducing damage into the substrate and are not backscattered like electron (Seliger *et al.* 1979). The ion energy is chosen as a compromise between the need to penetrate the resist (*ca.* 250 keV argon ions penetrate about 0.4 μm) and the need to avoid excessive damage to the substrate.

Ions are almost a hundred times more efficient for exposing resist than 20 keV electrons (Komura *et al.* 1979) because the energy of the ions is more completely absorbed in the resist layer. This high sensitivity can be a problem, however, for very high resolution because of inherent noise fluctuations created by the small number of ions needed to expose an image element. This is analogous to the situation for electron beam lithography discussed in §7.2.1. At an exposure dose of 10^{-8} C cm^{-2}, only 6 ions will expose a 0.1 μm × 0.1 μm element giving rise to a theoretical exposure uncertainty of 40%. Ten to a hundred times this exposure would be needed to reduce the uncertainty to the acceptable level of about 10%. This means that the minimum usable sensitivity for ions exposure is 10^{-7}–10^{-6} C cm^{-2}, that is about a tenth of that available with today's electron resists. Experiments have been carried out by Matsui *et al.* that show that PMMA lines 0.06 μm wide were continuous when there were 32 gallium ions per pixel (0.06 μm × 0.06 μm).

Even without the problem of statistical fluctuations the performance of ion-beam systems is marginal for economical exposure of resist because of ion opical constraints. The situation for other applications such as direct implantation or sputtering is no better because they require greater doses than resist exposure. In all cases, however, it may be practicable where the areas to be modified are a very small fraction of the sample area. This might be the case, for example, for selectively grading the channels of field-effect transistors.

8.3. *Ion sources and optics*

Two types of ion source produce high enough brightness (at least 10^6 A cm^{-2} sr^{-1}, 20 keV) to be considered for microfabrication; the field ion source (Hanson &

Siegel 1979) and the liquid metal source (Clampitt *et al.* 1975; Krohn & Ringo 1975). The field ion source produces relatively small energy spread (up to 3 eV) and when combined with a short focal length (up to 1 cm) electrostatic lens should provide a minimum beam size of about 10 nm with adequate current (10^{-11} A) for laboratory microfabrication experiments. This 10 nm is to be compared with less than 0.5 nm for electron beams where magnetic lenses with very short (less than 1 mm) focal length can be used.

The second type, the liquid metal source, produces higher currents and is more suitable for the larger beams needed for routine fabrication applications, but the energy spread is higher (10–12 eV), and the minimum beam diameter is about 100 nm. The relatively high brightnesses and beam currents reported for liquid metal sources are for gallium ions. Other species can be produced for ion implantation, or for greater penetration into resists, but only at lower brightness. Boron, arsenic and silicon ions are among the species that have been produced.

Electrostatic focusing and deflection must be used for ions and the systems that do this are at an earlier stage of development than the magnetic systems used for electrons. They are also more difficult to design because focusing and deflecting fields cannot be overlapped as they can with magnetic fields. Significant correction of aberrations has been accomplished for electrons by overlapping deflection and focusing. Multipole electrostatic lenses are used for focusing and deflecting high energy ion beams and some combination of these may offer a solution to this difficulty in the future but his is yet to be accomplished. In the absence of large aperture, wide angle, deflection, small fields can be tolerated by using similar techniques to those employed in small deflection field electron beam systems such as EBES. The sample is moved mechanically and laser interferometry is used to keep track of the sample position. Errors in position are corrected electronically by feeding signals to the beam deflection system.

Figure 23 shows the axial (undeflected) beam diameter against current for a high-performance ion probe that uses a liquid metal source. At beam currents of about 10^{-10} A, the beam size is 30–40 nm, which is comparable to that of the LaB_6 cathode electron beam system, but this electron beam system is designed for optimum operation at beam diameters of about 0.1 μm and currents between 10^{-7} and 10^{-8} A. Figure 24 shows that an electron-beam system suitable for nanolithography, with a shorter-focal-length lens, out-performs the ion beam system by producing a beam diameter of about 1 nm at 10^{-10} A.

8.4. *Resolution of ion beam processes*

Ultimately, resolution in a sputtering process is limited by ion penetration into the substrate and by the range over which the momentum can be transferred effectively enough to remove atoms from the sample surface. The diameter from which atoms can be sputtered has been reported to be about 10 nm for incident ion energies up to 12 keV (McHugh 1975). This means that it should be possible to fabricate structures of about 10 nm, which happens to be about the size of the smallest ion beam that can theoretically be produced with present ion sources (see figure 23). The smallest beams produced experimentally are about five times larger than this.

TABLE 4. RESOLUTION LIMITS AND THE FACTORS THAT DETERMINE THESE LIMITS FOR THE UV, X-RAY, ELECTRON AND ION BEAM LITHOGRAPHIES

lithography type	resolution limits: normal	resolution limits: ultimate
ultraviolet light contact proximity	2.5 μm Fresnel diffraction at minimum usable gap and wavelength $\lambda = 250$ nm, $t = 25$ μm	0.2 μm Fresnel diffraction contact print, resist thickness is 200 nm $\lambda = 200$ nm, $t = 200$ nm
X-ray proximity	0.2 μm Fresnel diffraction at usable gap for step and repeat operation $\lambda = 0.8$ nm, $t = 50$ μm	0.01 μm Fresnel diffraction and/or photoelectron range $\lambda = 4.4$ nm, $t = 25$ nm
optical projection	0.5 μm Fraunhofer diffraction at N.A. set by lens fabrication-field size constraints $\lambda = 250$ nm, N.A. = 0.4, depth of focus = 2 μm	0.2 μm Fraunhofer diffraction at wavelength set by absorption of resists and optical components $\lambda = 200$ nm N.A. = 0.9, depth of focus is 250 nm, field size is less than 200 μm
electron beam	<0.1 μm Resolution–throughput trade-off, and lateral scattering in normal resist thicknesses (>0.5 μm for $<\sim 30$ kV acceleration potential)	0.02 μm (conventional resist) delocalization of secondary electron exposure 0.001 μm (direct sublimation) combination of electron interaction range, and diffract spherical aberration
ion beam	<0.01μm resolution–throughput trade-off	0.02 μm (conventional resist) delocalization of secondary electron exposure 0.01 μm (direct milling) ion optical limits (chromatic aberration), sputter interaction range

For resist exposure, the resolution limit will be set by the range over which the ions interact with the resist. As with electron exposure, ion exposure will be delocalized by the creation of secondary electrons. Ultimate resolution will probably be 10–20 nm, as it is with electrons. At present this limit cannot be explored because the resolution of ion optical systems is inadequate.

8.5. *Summary*

Ion probes offer advantages for microanalysis and mask repair, but cannot yet compete with electron probes for microlithography, or nanolithography. The sources and lenses available today do not provide enough final beam current (more

than 0.1 μA) for the range of beam sizes (0.1–0.5 μm) needed for integrated circuit lithography, or small enough beam size (less than 2 nm) for nanolithography. The unfavourable comparison with electrons exists despite the fact that ions scatter over much smaller distances in the resist than electrons so there is no significant proximity effect, and that ions dissipate their energy more fully in the resist so the required exposure dose in coulombs per square centimetre is much lower.

Perhaps the greatest potential for ion beams lies in their use to directly modify materials. The much higher momentum of the ions compared to electrons should make then suitable for the type of processes discussed in section 7.3.2*b* which describes radiation damage lithography with electrons.

9. Conclusions

Table 4 summarizes, in abbreviated form, the resolution limits for the different lithographies, and the factors that set these limits. The highest-resolution method

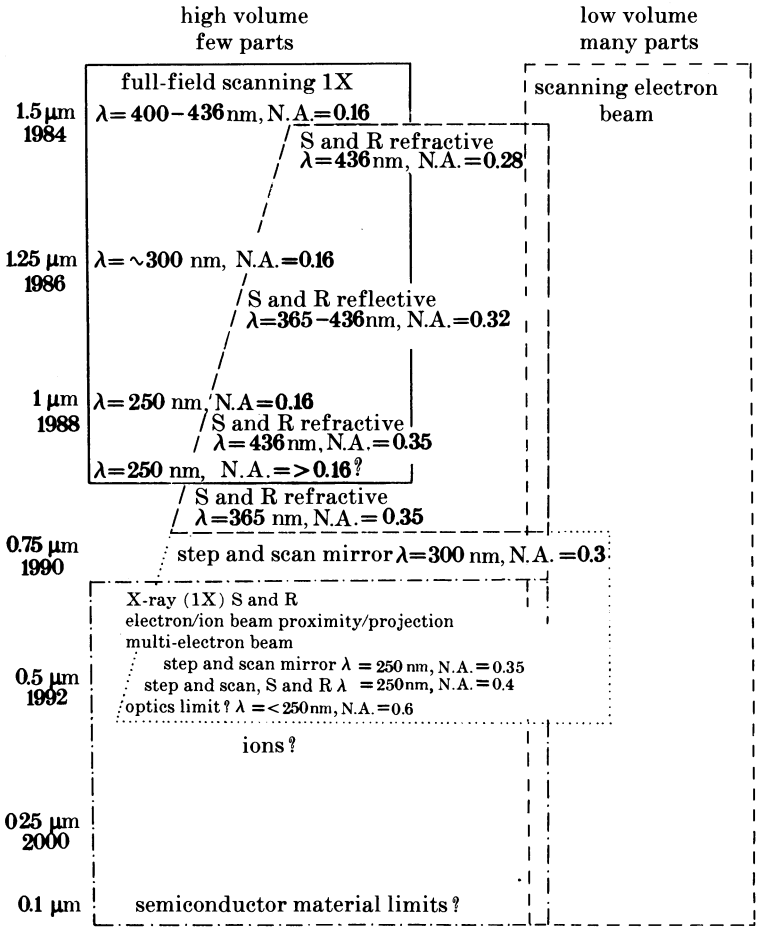

Figure 37. Possible sequence of implementation for the alternative lithographies for integrated circuit fabrication.

is electron-beam lithography and the smallest 'useful' structures made with this method are about 10 nm in size. Experimental electron-beam methods have been discovered that produce test structures about ten times smaller than this, but these methods have yet to be proven capable of making testable devices.

A possible sequence for the implementation of the different lithography methods for integrated circuit lithography is given in figure 37. It can be seen that there are many alternatives for the region below 0.5 μm and it is here that integrated circuit process engineers have to make their most difficult and most financially important decisions.

Much of what I have discussed has been the subject of two series of conferences; the European-based Microcircuit Engineering Conferences (*Microcircuit engineering*. London: Academic Press (1983, 1984, 1985, 1986)) and the USA-based International Symposia on Electron, Ion and Photon Beams (*J. Vac. Sci. Technol.* (1985, 1986, 1987)).

References

Alles, D. S., Biddick, C. J., Bruning, J. H., Clemens, J. T., Collier, R. J., Gere, E. A., Herriot, L. R., Leone, F., Liu, R., Mulrooney, T. J., Nielsen, R. J., Paras, N., Richman, R. M., Rose, C. M., Rosenfeld, D. P., Smith, D. E. A. & Thomson, M. G. R. 1987 *J. Vac. Sci. Technol.* B **5**, 47–52.

Broers, A. N. 1975 In *Scanning electron microscopy/1975* (ed. O. Johari & J. Corvin), pp. 661–670. Chicago: IIT Research Institute.

Broers, A. N. & Coane, P. A. 1986 *Appl. Phys. Lett.* **49**, 115–117.

Broers, A. N. & Laibowitz, R. B. 1978 In *Future trends in superconductive electronics* (ed. B. S. Deavor, Jr. *et al.*), pp. 289–297. New York: American Institute of Physics.

Broers, A. N. & Sedgwick, T. O. 1976 United States Patent 3971860.

Broers, A. N. 1965*a* *Electronics and reliability* vol. 4, pp. 103–104. Oxford: Pergamon Press.

Broers, A. N. 1965*b* Ph.D. thesis, University of Cambridge.

Broers, A. N. 1972 In *Proc. 5th Int. Conf. on Electron Ion Beam Science and Technology* (ed. R. Bakish), pp. 3–25. Princeton: Electrochemical Society Inc.

Broers, A. N. 1981 *J. electrochem. Soc.* **128**, 166–170.

Broers, A. N., Cuomo, J. J. & Krakow, W. 1981 IBM Technical Disclosure Bulletin vol. 24, pp. 1534.

Broers, A. N., Cuomo, J. J., Harper, J., Molzen, W., Laibowitz, R. B. & Pomerantz, M. 1978 *Electron microscopy 1978* (ed. J. M. Sturgess), vol. 111, pp. 343–354. Toronto: Microscopical Society of Canada.

Buckley, C. J., Browne, M. T. & Charalambous, P. 1985 *Proc. SPIE* **537**, 213.

Chang, T. H. P., Wilson, A. D., Speth, A. J. & Ting, C. H. 1976 In *Proc. 7th Int. Conf. Electron and Ion Beam Science and Technology* (ed. R. Bakish), pp. 392–406, Princeton: Electrochemical Society Inc.

Chang, T. H. P. 1975 *J. Vac. Sci. Technol.* **12**, 1271–1275.

Chaudhari, P., Broers, A. N., Chi, C. C., Laibowitz, R. B., Spiller, E. & Viggiano, J. 1980 *Phys. Rev. Lett.* **45**, 930–932.

Clampitt, R., Aitken, K. L. & Jeffries, D. K. 1975 *J. Vac. Sci. Technol.* **12**, 1208.

Essig, M. & Pfeiffer, H. C. 1986 *J. Vac. Sci. Technol.* B**4**, 83–85.

Everhart, T. E. 1984 In *Materials in microlithography* (ed. L. F. Thompson, C. G. Willson & J. M. J. Frechet), pp. 5–9. Washington, D.C.: American Chemical Society.

Goto, E., Soma, T. & Idesawa, M. 1978 *J. Vac. Sci. Technol.* **15**, 883–886.

Greed, J. A. & Markle, D. A. 1982 In *Optical microlithography* (*Proc. SPIE*) **334**, 2–9.

Gruen, A. E. 1957 *Z. Naturf.* A**12**, 89–95.

Hanson, G. R. & Siegel, B. M. 1979 *J. Vac. Sci. Technol.* **16**, 1875–1878.

Hatzakis, M. *et al.* 1980 *IBM J. Res. Dev.* **14**, 452.

Herriott, D. R., Collier, R. J., Alles, D. S. & Stafford, J. W. 1975 *IEEE Trans. Electron Devices* **ED-22**, 385–392.

PROCEEDINGS OF THE ROYAL SOCIETY A MATHEMATICAL, PHYSICAL & ENGINEERING SCIENCES

Hershel, R. & Voison, R. 1982 *Photogr. Sci. Engng* **334**, 44–51.
Heuberger, A. 1986*a* In *Microcircuit engineering* vol. 86, pp. 3–38. Amsterdam: North-Holland.
Heuberger, A. 1986*b* *Solid State Technol.* **29–2**, 93–101.
Howard, R. E., Jackel, J. D. & Skocpol, W. J. 1985 In *Microcircuit engineering* vol. 85, pp. 3–16. Amsterdam: North-Holland.
Hsia, L. C. & Weber, E. V. 1985 *J. Vac. Sci. Technol.* B **3**, 128–130.
Isaacson, M. & Muray, A. 1981 *J. Vac. Sci. Technol.* **19**, 1117–1120.
Jain, K., Willson, C. G. & Lin, B. J. 1982 *IEEE Trans. Electron Device Lett.* **EDL-3**, 53–55.
Jones, G. A. C., Blythe, S. & Ahmed, H. 1986 In *Microcircuit engineering 86*, pp. 265–271. Amsterdam: North-Holland.
Kern, D. P., Sturans, M. A., Pfeiffer, H. C. & Stickel, W. 1984 In *Microcircuit Engineering 84* (ed. A. Heuberger, & H. Beneking), pp. 185–194. London: Academic Press.
King, H. J., Merritt, P. E., Otto, O. W., Ozdemir, F. S., Pasiecznik, J., Carroll, A. M., Caran, D. L., Eckes, W., Lin, L. H., Veneklasen, L. & Wiesner, J. C. 1985 *J. Vac. Sci. Technol.* B **3**, 106–111.
King, M. C. 1981 In *Principles of optical lithography* (ed. N. G. Einsbruch) vol. 1, pp. 2–81. Academic Press: New York, London, Toronto, Sydney and San Francisco.
Komura, M., Atoda, N. & Kawakatsu, H. 1979 *J. electrochem. Soc.* **126**, 483.
Kratschmer, E. & Isaacson, M. 1986 *J. Vac. Sci. Technol.* B **4**, 361–364.
Krohn, V. E. & Ringo, G. R. 1975 *Appl. Phys. Lett.* **27**, 479–481.
Laibowitz, R. B., Broers, A. N., Yeh, J. T. C. & Viggiano, J. M. 1979 *Appl. Phys. Lett.* **35**, 891–893.
Lin, B. J. 1979 *Photogr. Sci. Engng* **23 (6)**, 174.
Mackie, W. S., Patrick, W., Beaumont, S. P. & Wilkinson, C. D. W. 1985 In *Microcircuit engineering 84*, pp. 213–218. London: Academic Press.
Markle, D. A. 1984 *Solid State Technol.* **27 (9)**, 159.
Matsui, S., Mori, K., Saigo, K., Shiokawa, T., Toyoda, K. & Namba, S. 1986 *J. Vac. Sci. Technol.* B **4**, 845–849.
Mayadas, A. F. & Laibowitz, R. B. 1972 *Phys. Rev. Lett.* **28**, 156–158.
McHugh, J. A. 1975 In *Methods of surface analysis* (ed. S. Wolsky & A. Czanderna). Amsterdam: Elsevier.
Mochel, M. E., Humphreys, C. J., Mochel, J. M. & Eades, J. A. 1983 In *Proc. 41st Annual Meeting of the Electron Microscopy Society of America*, pp. 100–101. San Francisco Press.
Mollenstedt, G. & Speidel, R. 1960 *Phys. Bl.* **16**, 192.
Moore, R. D., Caccoma, G. A., Pfeiffer, H. C., Weber, E. V. & Woodward, O. C. 1981 *J. Vac. Sci. Technol.* **19**, 950–952.
Newman, T. H., Williams, K. E. & Pease, R. F. W. 1987 *J. Vac. Sci. Techol.* B **5**, 88–91.
Offner, A. 1979 *Photogr. Sci. Engng* **23 (6)**, 374.
Palma, E. J. & Hart, R. R. 1987 *J. Vac. Sci. Technol.* B **5**, 228–231.
Pfeiffer, H. C. 1978 *J. Vac. Sci. Technol.* **15**, 887–890.
Pfeiffer, H. C. 1979 *IEEE Trans. Electron. Dev.* **ED-26**, 663–674.
Pol, V. 1987 *Solid State Technol.* **30–1**, 71–76.
Sedgwick, T. O., Broers, A. N. & Agule, B. J. 1972 *J. electrochem. Soc.* **199**, 1769–1771.
Seliger, R. L., Kubena, R. D., Olney, R. D., Ward, J. W. & Wang, V. 1979 *J. Vac. Sci. Technol.* **16**, 1610–1612.
Spears, D. L. & Smith, H. I. 1972 *Electron. Lett.* **8**, 102–104.
Spiller, E. & Feder, R. 1977 In *X-ray optics-applications to solids* (ed. Queisser, H. J.), pp. 35–92. Berlin and New York: Springer-Verlag.
Tai, K. L., Sinclair, W. R., Vadinsky, R. J. & Moran, J. M. 1979 *J. Vac. Sci. Technol.* **16**, 1977–1979.
Thomson, M. G. R., Collier, R. J. & Herriott, D. R. 1978 *J. Vac. Sci. Technol.* **15**, 891–895.
Van der Mast, K. D., Jansen, J. H. & Barth, J. E. 1985 In *Microcircuit engineering 85*, pp. 43–51. Amsterdam: North-Holland.
Varnell, G., Spicer, D. F., Hebley, J., Robbins, R., Carpenter, C. & Malone, M. 1979 *J. Vac. Sci. Technol.* **16**, 1787–1793.
Voss, R., Laibowitz, R. B. & Broers, A. N. 1980 *Appl. Phys. Lett.* **37**, 656–658.
Ward, R., Franklin, A. R., Lewin, I. H., Gould, P. A. & Plummer, M. J. 1986 *J. Vac. Sci. Technol.* **B4**, 89–93.

PROCEEDINGS OF THE ROYAL SOCIETY A MATHEMATICAL, PHYSICAL & ENGINEERING SCIENCES

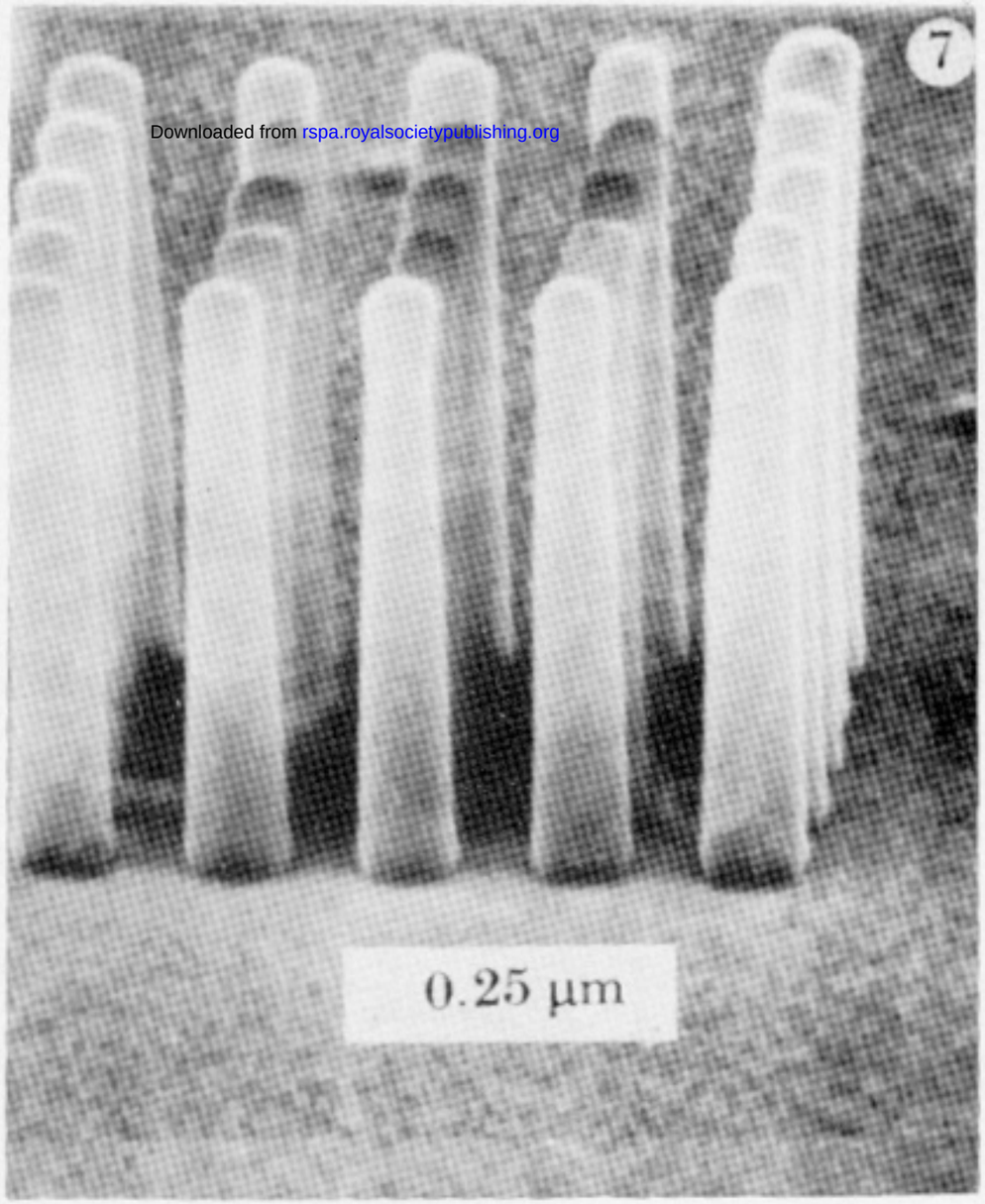

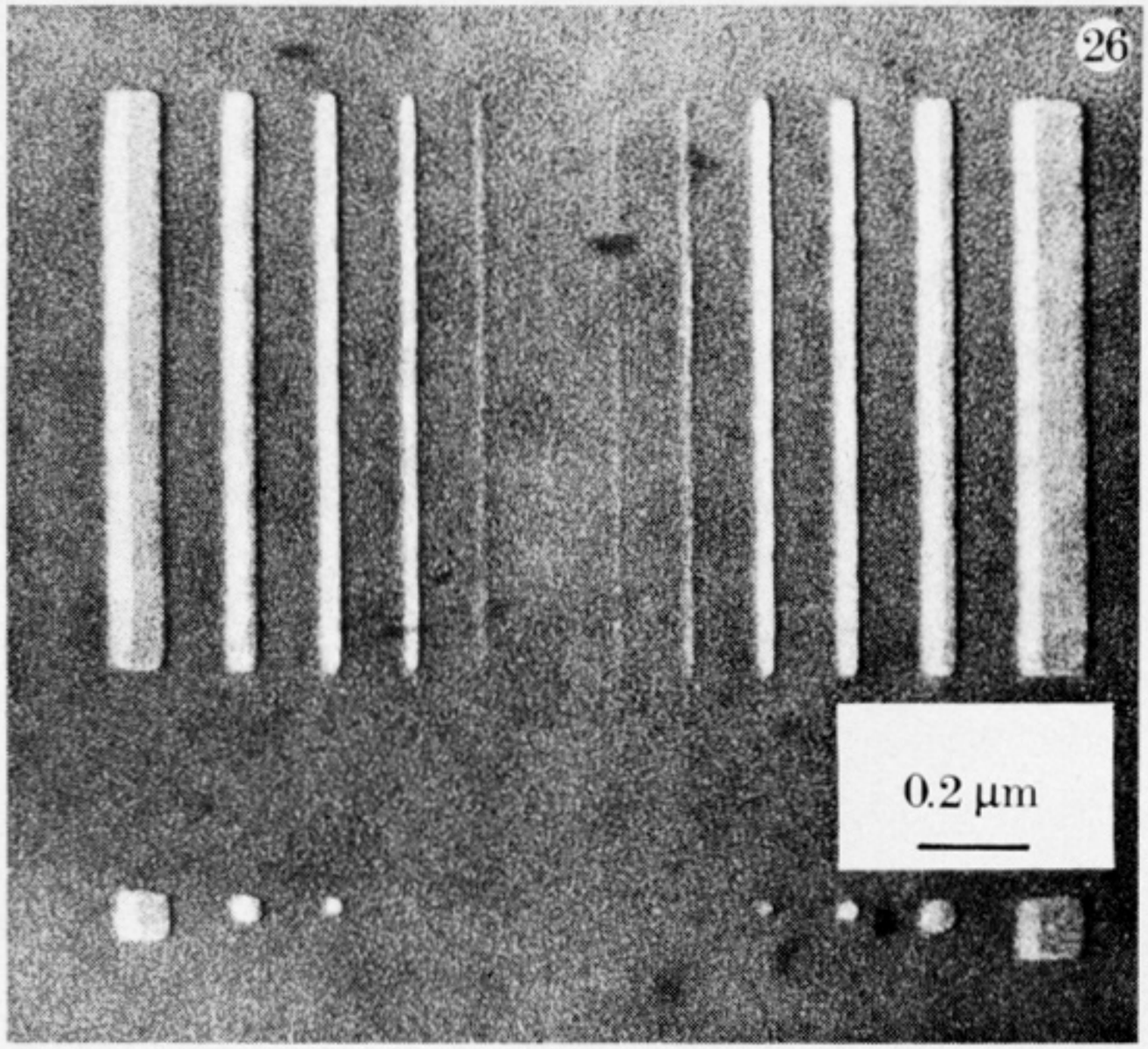

FIGURE 7. High-aspect-ratio resist patterns fabricated with X-ray lithography (Heuberger 1987*b*).

FIGURE 26. One of a series of test patterns used to measure the resolution of electron resist (Broers 1981). The 60 nm thick PMMA resist layer is supported on a 60 nm thick Si_3N_4 membrane and the pattern has been exposed with a 0.5 nm diameter 50 kV electron beam. The sample has been shadowed at 45° with AuPd to highlight the structure and to reveal the resist thickness. This particular exposure is made at a slightly larger dose than is needed to open up the largest shapes in the pattern.

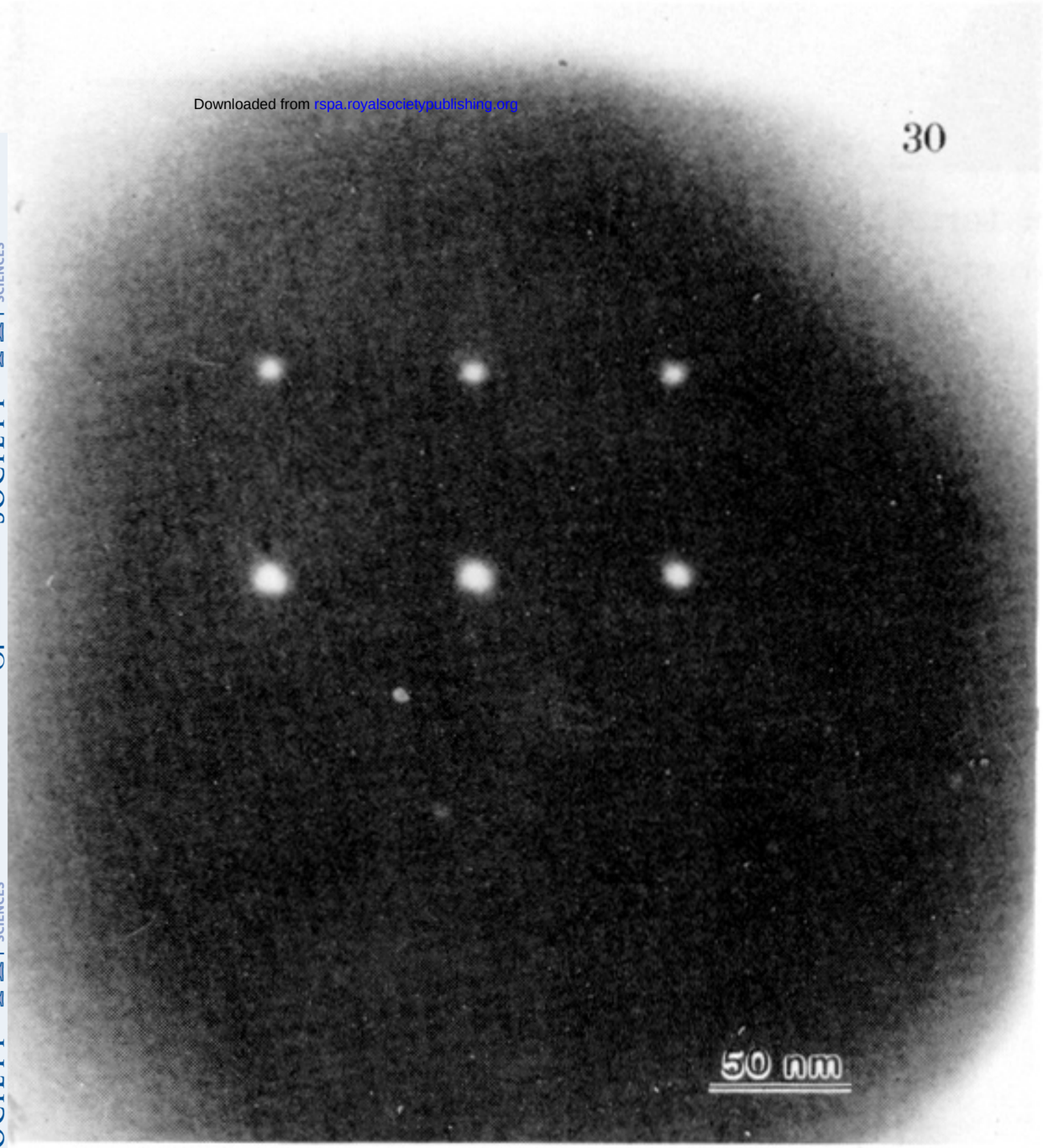

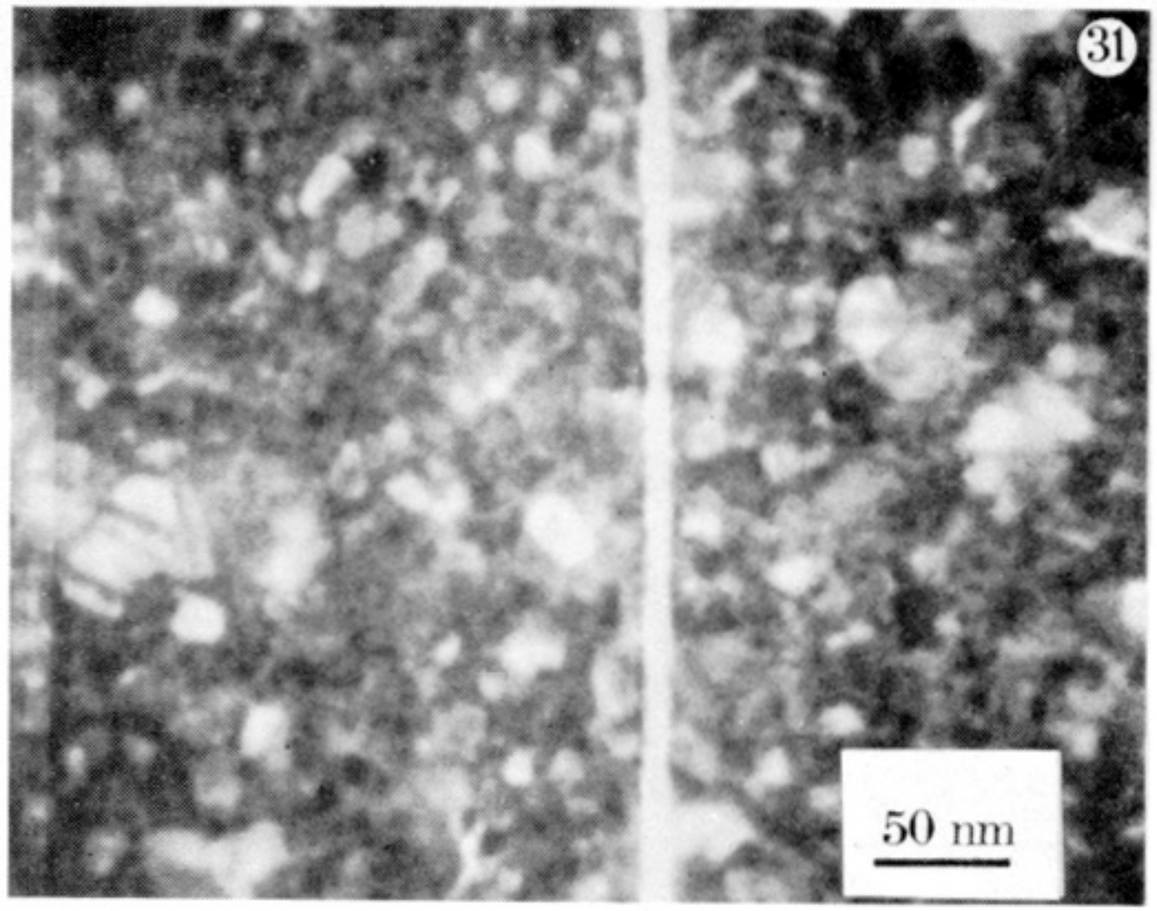

FIGURE 30. 5 nm diameter holes drilled in NaCl with 1 nm diameter electron beam (Broers *et al.* 1978).

FIGURE 31. A 10 nm wide slot ion milled in a 20 nm thick gold film using directly patterned MgF_2 as a mask.

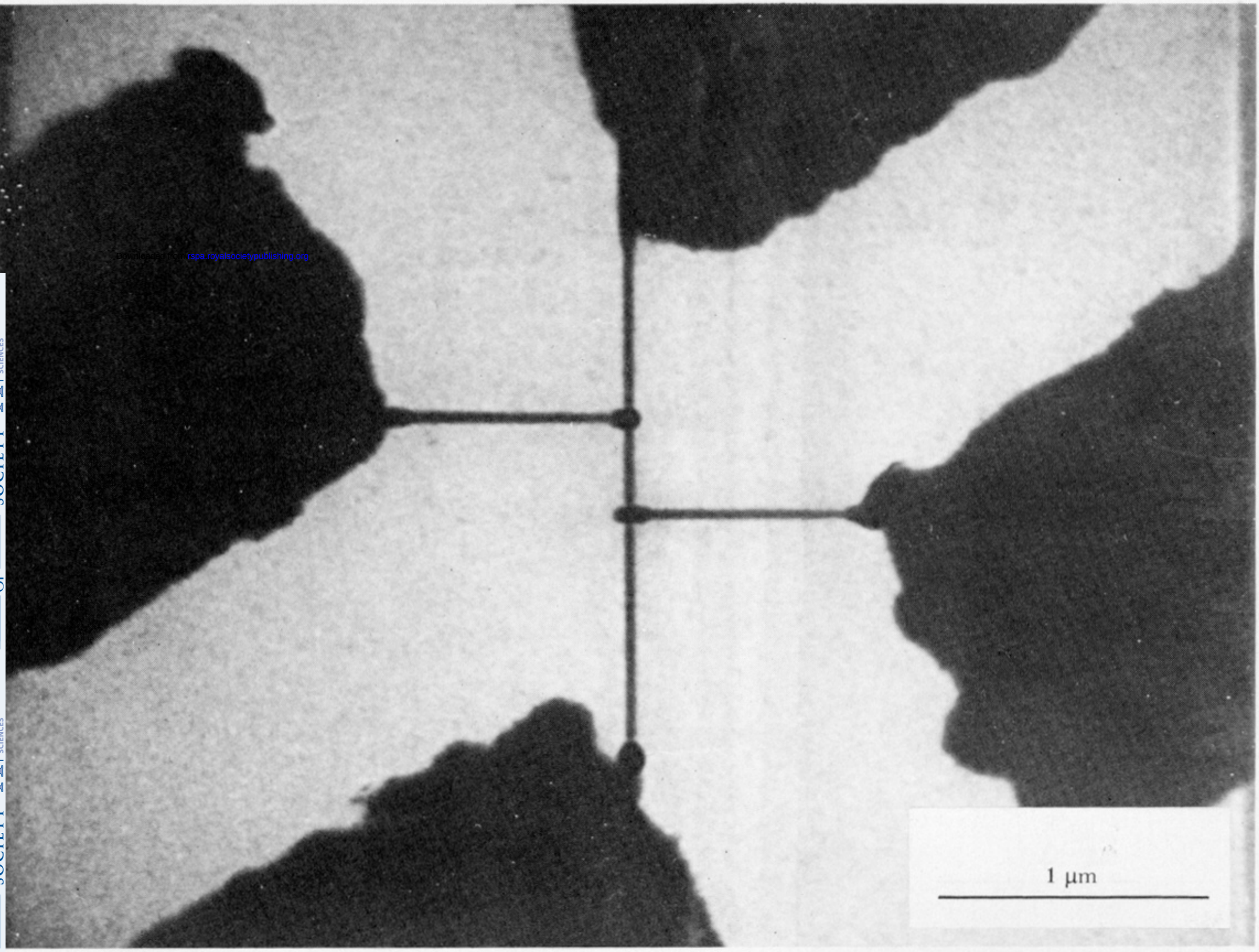

FIGURE 36. 25 nm wide niobium wires in a four-terminal configuration used for exploring localization effects (Laibowitz *et al.* 1979).

PROCEEDINGS OF THE ROYAL SOCIETY A MATHEMATICAL, PHYSICAL & ENGINEERING SCIENCES